



1 Distinct dual-isotopic signatures of major methane sources in South Asia

2 Peng Yao¹, Katja Belec¹, Henry Holmstrand¹, Josh Balacky¹, Abdus Salam², Krishnakant
3 Budhavant^{3,4}, Mohanan Remani Manoj¹, Khaled Shaifullah Joy^{2,5}, Md. Alamin Hossain²,
4 Atinderpal Singh⁶, Anil Patel^{7,8,9}, Neeraj Rastogi⁷, Chinmay Mallik¹⁰, Kirpa Ram¹¹, Gyanesh
5 Kumar Singh^{12,13}, Örjan Gustafsson*¹

6 ¹Department of Environmental Science (ACES) and the Bolin Centre for Climate Research,
7 Stockholm University, Stockholm 10691, Sweden

8 ²Department of Chemistry, University of Dhaka, Dhaka 1000, Bangladesh

9 ³Divecha Centre for Climate Change, Indian Institute of Science, Bangalore 560012, India

10 ⁴Maldives Climate Observatory-Hanimaadhoo (MCOH), Maldives Meteorological Services, H.
11 Dh. Hanimaadhoo 02020, Maldives

12 ⁵Department of Chemistry, Drexel University, Philadelphia, PA-19104, United States

13 ⁶Department of Environmental Studies, University of Delhi, Delhi, 110007, India

14 ⁷Geosciences Division, Physical Research Laboratory, Ahmedabad 380009, India

15 ⁸Bagchi School of Public Health, Ahmedabad University, Ahmedabad 380009, Gujarat, India

16 ⁹The Climate Institute, Ahmedabad University, Ahmedabad 380009, Gujarat, India

17 ¹⁰Department of Atmospheric Science, Central University of Rajasthan, Ajmer 305801, India

18 ¹¹Department of Chemistry, Institute of Science, Banaras Hindu University, Varanasi 221005,
19 India

20 ¹²Department of Civil Engineering, Indian Institute of Technology Kanpur, Kanpur, 208016, India

21 ¹³Air Quality and Aerosol Metrology (AQAM) Group, National Physical Laboratory (NPL),
22 Teddington, London TW11 0LW, UK

23 Corresponding: Örjan Gustafsson (Orjan.Gustafsson@aces.su.se)

24



25 **Abstract**

26 Methane is a powerful greenhouse gas contributing significantly to global warming. South Asia is
27 a major methane emission region, yet source-diagnostic isotopic signatures remain poorly
28 constrained, limiting top-down source attribution. To address this gap, we conducted extensive
29 sampling and isotopic analyses of major methane sources in South Asia. Our results reveal
30 substantial deviations of South Asian methane source fingerprints from global means. Methane
31 from C3 biomass burning is more depleted in $\delta^{13}\text{C}$ ($-30.9\pm2.2\text{\textperthousand}$) but more enriched in $\delta^2\text{H}$ ($-$
32 $201\pm18\text{\textperthousand}$), while ruminant methane (C3) is strongly depleted in both $\delta^{13}\text{C}$ ($-68.7\pm0.5\text{\textperthousand}$) and $\delta^2\text{H}$
33 ($-343\pm6\text{\textperthousand}$). In contrast, rice paddy methane is more enriched in $\delta^{13}\text{C}$ ($-53.8\pm0.8\text{\textperthousand}$) and $\delta^2\text{H}$ ($-$
34 $311\pm6\text{\textperthousand}$), with their ratios signaling pre-emission oxidation. Wastewater methane shows enriched
35 $\delta^{13}\text{C}$ ($-45.0\pm2.4\text{\textperthousand}$) and depleted $\delta^2\text{H}$ ($-350\pm10\text{\textperthousand}$) relative to global means, with minimal
36 oxidation or spatial variation. These pronounced regional differences highlight the importance of
37 using regionally constrained source fingerprints in isotope-based source apportionment. A global
38 synthesis further shows that $\delta^{13}\text{C}$ signatures of biomass burning and ruminant methane are
39 primarily controlled by C3/C4 feedstocks, whereas $\delta^2\text{H}$ is relatively insensitive to substrate type.
40 Methane from rice paddies and wetlands exhibits strong latitudinal gradients worldwide.
41 Combining emission inventories with source-specific isotope fingerprints reveals a mismatch with
42 atmospheric methane in South Asia, suggesting an overestimation of rice paddy emissions and/or
43 an underestimation of other microbial sources. These findings demonstrate the utility of top-down
44 dual-isotope constraints to refine regional methane budgets and mitigation strategies.

45 **Keywords:** biomass burning, ruminant, rice paddy, wastewater



47 **1. Introduction**

48 Mitigating methane emissions is critical for achieving the Paris Agreement 2°C target (e.g.,
49 (Rogelj et al., 2016)). Methane (CH_4) is a potent greenhouse gas (GHG) with a 20-year global
50 warming potential 84 times that of an equal mass of CO_2 , contributing ~20% to total global
51 warming (Naik et al., 2023). Despite its significance, the drivers of recent methane increases
52 remain uncertain (Nisbet et al., 2023; Schaeffer et al., 2025), highlighting the need for precise
53 monitoring and effective mitigation strategies. Anthropogenic emissions are major contributors
54 (Bousquet et al., 2006; Zhang et al., 2022; Saunois et al., 2025) and understanding methane sources
55 and sinks is essential for targeted reduction efforts. The tropics, particularly South Asia, account
56 for an estimated ~60% of global methane emissions (Jackson et al., 2020; Feng et al., 2022;
57 Saunois et al., 2025). South Asia is one of the largest and fastest-growing methane emitters, with
58 contributions believed to be primarily from anthropogenic sources (Stavert et al., 2022). The
59 region experiences extensive biomass burning (Kirschke et al., 2013), hosts the world's largest
60 ruminant population (Ganesan et al., 2017), is a major rice producer (Singh et al., 2021) and has
61 substantial waste emissions from the dense population (Chakraborty et al., 2011). However,
62 methane source apportionment and quantification in this region is limited and remain highly
63 uncertain.

64 Methane sources are broadly classified as microbial, combustion and thermogenic (Whiticar,
65 1999). Microbial sources include e.g., wetlands, rice paddies, ruminants, landfills and wastewater
66 (Masson-Delmotte et al., 2021). Combustion sources of methane is believed to be dominated by
67 biomass burning emissions but also include coal combustion, traffic emissions and other
68 combustion processes (Saunois et al., 2025). Thermogenic methane originates from fugitive
69 emissions during fossil fuel extraction, transport and processing (Sherwood et al., 2017; Menoud



70 et al., 2022). The spatial and temporal variability of these sources, coupled with the atmosphere's
71 open system, introduces substantial uncertainties in methane estimates (Saunois et al., 2025).
72 Bottom-up estimates of methane emissions remain uncertain due to varying methodologies and
73 biases across different source sectors (Zavala-Araiza et al., 2015; Hristov et al., 2017). Recent
74 satellite-based top-down observations have helped to improve some estimates (Lauvaux et al.,
75 2022; Shen et al., 2023; Cusworth et al., 2024), yet are challenged by dispersed sources such as
76 from ruminants and waste that are distributed through the landscape.

77 Estimates of methane emissions based on isotopic constraints are promising for fingerprinting the
78 relative source contributions in an intercepted receptor setting, yet remain limited by uncertainties
79 in both source-specific isotopic signatures and in atmospheric sinks. Moreover, large-scale top-
80 down isotopic observations are lacking. Nevertheless, isotopic analysis can be a powerful tool for
81 not only the source attribution but also for quantification of their reaction sinks (Fischer et al.,
82 2008; Bock et al., 2017; Dyonisius et al., 2020; Nisbet et al., 2023). However, methane isotopic
83 studies in South Asia remain highly limited (Rao et al., 2008; Metya et al., 2022), with isotopic
84 source signatures nearly completely lacking (Metya et al., 2022). Establishing regional isotopic
85 source signatures is critical for achieving source apportionment and reducing uncertainties in
86 estimates of methane emissions.

87 In this study, we analyzed $\delta^{13}\text{C}$ and $\delta^2\text{H}$ signatures from four key methane emitting sources in
88 South Asia, namely biomass burning, ruminants, rice paddies and wastewater. By evaluating
89 isotopic variability across emission processes, sampling techniques and geographic regions, this
90 work aims to constrain methane isotopic source signatures and thereby facilitate subsequent top-
91 down isotope-based source apportionment to reduce uncertainties in methane emissions. A global



92 review of methane isotopic values was further conducted to compare with those of these herewith
93 constrained South Asian sources.

94

95 2. Materials and Methods

96 2.1. Gaseous and aqueous methane source sampling

97 Cattle ruminant samples in South Asia were collected using a custom-built sampling instrument.
98 Sample air was passed through magnesium perchlorate (CAS# 10034-81-8, Alfa Aesar) to
99 remove moisture, into an electrically-powered membrane pump (KNF Neuberger N86), and out
100 into two cylindrical 1000 mL borosilicate 3.3 glass flasks (Normag, Germany) with axial inlet and
101 outlet, connected in series. The inlet and outlet of each flask were sealed with a Normag needle
102 valve with high-diffusion-minimized sealing. Tubing was made of PTFE and Synflex(R) and
103 connections were Swagelok(R) and UltraTorr (TM). The flasks were pre-conditioned with clean
104 air to eliminate contaminants. Before sampling, the flasks were conditioned in a 4-step protocol:
105 Evacuated at high vacuum at 50°C for 12h, purged with nitrogen at 50°C for 2h, again evacuated
106 at high vacuum at 50°C, for 3h, and finally filled with pre-conditioned clean air to a pressure of
107 1.3 bar (absolute). Sampling was conducted by positioning a funnel 2–5 cm from the cattle's
108 mouths to capture their breath. The sample air was pumped through the flasks for 5 min, then
109 closing the outlet valve and letting pressure build up to 1.7 bar (absolute), after which the flask
110 valves were closed. Finally, flask in- and outlets were sealed with parafilm to prevent
111 contamination from dust etc.

112 For combustion sources, we collected exhaust samples from agricultural crop residue burning in
113 South Asian fields using the same custom-built instrument. Sampling was performed 3–15 cm



114 from the burning rice paddies. A 0.45 μm inline gas filter was placed between the PTFE tubing
115 and the metal tubing to remove aerosols. Each sampling session lasted 5 minutes, with the final
116 flask pressure reaching 1.2 bar (absolute).

117 Samples were also collected to constrain the isotope fingerprints of aqueous microbial sources in
118 South Asia, including rice paddies and wastewater. Rice paddy sampling involved dividing each
119 paddy into four quadrants and taking one to three replicate samples from the center of each
120 quadrant, totaling 4-12 samples per paddy field. For wastewater, three replicate samples were
121 collected from sewage at each location. Before sampling, glass vials (VMR) were rinsed thrice
122 with 125 mL of either rice paddy water or wastewater. Samples were then collected by submerging
123 the vials to mid-depth for 20 seconds until bubbling ceased, followed by an additional five-second
124 hold. The vials were then sealed with a bromine butyl rubber stopper (Apodan Nordic) attached to
125 a string. After sampling, 0.5 mL of saturated ZnCl_2 solution was added as a preservative, and the
126 vials were crimp-sealed, labeled, and stored at 4 °C in the dark before and after being shipped to
127 Stockholm University for further analysis.

128 Thus, we collected a substantial number of methane samples from the four sources: ruminants,
129 biomass burning, rice paddies and wastewater (see Supplementary Data S1 for details of each
130 sample). Among them, ruminants and biomass burning represent two major sources of gaseous
131 methane, while rice paddies and wastewater are significant atmospheric sources of aqueous,
132 dissolved methane. The ruminant samples were obtained from 6 farms across South Asia, totaling
133 40 samples. For biomass burning, we conducted 4 sampling campaigns in different regions,
134 collecting a total of 17 samples. Rice paddy samples were collected from 18 different rice-growing
135 areas, amounting to 185 samples. Wastewater samples were gathered from 13 sewage treatment
136 plants, totaling 38 samples. The sample distribution is illustrated in Fig. 1, with gaseous methane



137 samples from biomass burning and ruminants primarily collected in Bangladesh, while aqueous
138 methane samples from rice paddies and wastewater are distributed across Bangladesh and several
139 densely populated regions of India. The background color of Fig. 1 represents total methane fluxes
140 in 2023, sourced from EDGAR (Crippa et al., 2021), indicating significant methane emissions in
141 South Asia.

142

143 **2.2. Analysis of methane mixing ratios and isotopic composition**

144 Methane mixing ratios were measured using gas chromatography with flame ionization detection
145 (GC-FID, Agilent Technologies 7890A). For gaseous source samples, methane was extracted from
146 a glass flask using a syringe and injected directly into the instrument. For aqueous source samples,
147 a portion of the liquid was extracted, and helium (He) was introduced. After equilibration, a syringe
148 was used to collect the headspace mixture of helium, methane and other dissolved gases for
149 analysis. Three methane standards with methane concentrations of 1.6 ppm, 80.3 ppm and 250
150 ppm in synthetic air were used for calibration.

151 The equilibrium between the gaseous and aqueous phases was evaluated using Henry's Law
152 (equation 1):

$$153 \quad c = k \times P \quad (1)$$

154 where c is the concentration of dissolved methane (nmol L^{-1}), k is Henry's law constant, and P is
155 the partial pressure of methane. For the calculations: the water volume was 40 mL, the headspace
156 volume was 10 mL, the headspace pressure was 1 atm, the equilibration temperature was 25°C,



157 the gas constant R was $0.08025 \text{ atm}\cdot\text{L mol}^{-1}\cdot\text{K}^{-1}$, and Henry's Law constant k for methane at 25°C
158 was $0.0014 \text{ mol L}^{-1} \text{ atm}^{-1}$.

159 Once the methane mixing ratios were determined, gaseous and aqueous source samples were
160 analyzed for $\delta^{13}\text{C}$ and $\delta^2\text{H}$ using gas chromatography isotope ratio mass spectrometry (GC-IRMS;
161 Delta V Plus, Thermo Fisher). Due to variable methane mixing ratios in source samples, two
162 methods were used: pre-concentration (Precon) for diluted samples (Rice et al., 2001) and direct
163 injection, using the GC injector, for concentrated samples. The Precon system was modified with
164 custom-built components to improve isotopic analysis. In this configuration, only liquid nitrogen
165 was used as the cryogen for all traps. CO_2 and water vapor were first removed with chemical
166 absorbents, followed by Trap 1 for additional purification. Trap 2 (a 1/8" stainless steel tube, 20
167 cm in length, packed with HayeSep D, mesh size ##) was then employed, with sufficient venting
168 through the Precon six-port valve to remove most of the residual oxygen that could interfere with
169 $\delta^2\text{H}$ measurements. The sample was subsequently transferred to Trap 3 (a PoraPLOT capillary,
170 0.32 mm internal diameter), and final separation was performed on a $5 \text{ m} \times 0.32 \text{ mm}$ PoraPLOT
171 column at -78°C (dry ice). This procedure ensured effective resolution of the methane peak from
172 any remaining oxygen before conversion in the high-temperature reactor. Any interference by
173 krypton (Kr) in the $\delta^{13}\text{C}$ analysis was eliminated by post-column GC separation from the methane-
174 derived carbon dioxide peak (PoraPLOT 7 m \times 0.32 mm; (Schmitt et al., 2013)). To match the
175 relatively narrow detection range of the IRMS, syringe dilutions with He were applied. Isotopic
176 values were corrected for instrumental drift and calibrated using standards.

177 Isotope values are reported in δ notation, representing the relative deviation of isotope abundance
178 in a sample compared to international standards: Vienna Pee Dee Belemnite (V-PDB) for $\delta^{13}\text{C}$ and
179 Vienna Standard Mean Ocean Water (V-SMOW) for $\delta^2\text{H}$. For diluted samples, the two standards



180 used were both 1.85 ppm, with $\delta^{13}\text{C}$ values of $-48.4\pm0.3\text{\textperthousand}$ and $-68.6\pm0.3\text{\textperthousand}$, and $\delta^2\text{H}$ values of
181 $-63\pm5\text{\textperthousand}$ and $-240\pm5\text{\textperthousand}$. For concentrated samples, $\delta^{13}\text{C}$ was measured directly using a 100-ppm
182 standard with a $\delta^{13}\text{C}$ value of $-43.8\text{\textperthousand}$, while $\delta^2\text{H}$ was measured after pre-dilution and corrected
183 using the same approach as for diluted samples. Analytical uncertainties of the reported isotopic
184 composition are $0.09\text{\textperthousand}$ for $\delta^{13}\text{C}$ and $2.1\text{\textperthousand}$ for $\delta^2\text{H}$. The here constrained isotopic data of the major
185 methane sources in South Asia are summarized in Supplementary Data S1.

186

187 **2.3. Determination of isotopic source signatures**

188 To determine the isotopic values of the sources, we analyzed the isotopic data for all samples using
189 the Keeling (Keeling, 1958; Pataki et al., 2003) and Miller-Tans (Miller and Tans, 2003) methods.
190 These approaches follow the equations 2 and 3:

$$191 \quad \delta^{13}\text{C}_{obs} = c_{bg} \times (\delta^{13}\text{C}_{bg} - \delta^{13}\text{C}_{source}) \times \frac{1}{c_{obs}} + \delta^{13}\text{C}_{source} \quad (2)$$

$$192 \quad \delta^{13}\text{C}_{obs} \cdot c_{obs} - \delta^{13}\text{C}_{bg} \cdot c_{bg} = \delta^{13}\text{C}_{source} \cdot (c_{obs} - c_{bg}) \quad (3)$$

193 where c represents the CH_4 mixing ratio, and the subscripts obs , bg , and $source$ denote atmospheric
194 observations, background levels, and source contributions, respectively. The Miller-Tans
195 approach, which yielded narrow uncertainties, was used in the main text, while the Keeling plots
196 are provided as additional information in Supplementary Figs. S1–S4.

197 We employed Kriging interpolation using the *gstat* package in R to evaluate the spatial distribution
198 of isotopic values. This geostatistical method estimates values at unsampled locations based on the
199 spatial autocorrelation of observed data, modeled through a fitted variogram. We applied this



200 approach to interpolate $\delta^2\text{H}$ values of global surface water and representative microbial methane
201 sources (ruminants, wetlands and rice paddies, and waste) for comparative spatial analysis.

202 To calculate methane isotopic source signatures and integrate contributions from multiple sources,
203 we used a combination of statistical approaches. Uncertainty propagation was quantified using
204 Monte Carlo simulations (10,000 iterations), accounting for variability in both isotopic
205 measurements and source fractions.

206

207 **2.4. Literature review of isotopic signatures of global methane sources**

208 A comprehensive literature review was conducted to compile isotopic source signatures, which
209 were further assessed for major global and regional methane sources (Supplementary Data S2).
210 The review was carefully curated to minimize the influence of individual studies by selecting only
211 a single representative value per region from each publication. Source-specific mathematical
212 approaches were applied, as detailed in the following sections.

213 In the final section, we integrated the synthesized isotopic signatures with a range of top-down and
214 bottom-up estimates to evaluate the discrepancies between current emission inventories and
215 isotopic source constraints. Global data were compiled from our extensive literature review (Data
216 S2). Isotopic values for microbial sources were calculated using Monte Carlo simulations,
217 integrating our findings with estimates from Saunois et al. (2025) (Saunois et al., 2025), Ito et al.
218 (2023) (Ito et al., 2023), and the IPCC (Masson-Delmotte et al., 2021) assessment. For South Asia,
219 we incorporated isotopic signatures of rice paddy methane, while for natural wetlands, we retained
220 tropical region values from the global review, as there is no evidence indicating significant
221 methane oxidation in South Asian wetlands. Thermogenic methane isotopic values were sourced



222 from extensive global (Sherwood et al., 2017) and European (Menoud et al., 2022) databases. The
223 South Asian dataset focuses on methane sources across Afghanistan, Bangladesh, India and
224 Pakistan. Thermogenic methane primarily originates from natural gas, coalbed methane, shale gas
225 and other methane emissions associated with fossil fuel extraction, transportation and processing.
226 This thermogenic category also includes minor contributions from biogenic methane present in
227 various mineral deposits, incorporated to facilitate the source analysis of atmospheric methane.

228

229 **3. Results and discussion**

230 **3.1. Methane from agricultural biomass burning**

231 The isotopic source signatures of methane from agricultural biomass burning in South Asia was
232 constrained and compared to measurements elsewhere (Fig. 2, Table 1, Supplementary Data S1–
233 S2) to establish robust and representative source end-member values. The $\delta^{13}\text{C}$ and $\delta^2\text{H}$ values
234 derived from Miller–Tans plots (Fig. 2A–2B) were $-30.9\pm2.2\text{‰}$ and $-201\pm18\text{‰}$, respectively.
235 Keeling plots yielded comparable $\delta^{13}\text{C}$ values but slightly more enriched $\delta^2\text{H}$ values
236 (Supplementary Fig. S1). The Keeling plot is mathematically rigorous, whereas the Miller–Tans
237 method is empirical. The Keeling plot requires a more pronounced perturbation against a stable
238 background, while the Miller–Tans method is more sensitive and provides more reliable estimates
239 under weaker perturbations. In this study, we applied the more sensitive Miller–Tans method to
240 account for a wide range of conditions. In these sampling campaigns, methane primarily originated
241 from agricultural crop residue burning of C3 biomass. The linear relationship between $\delta^2\text{H}$ versus
242 $\delta^{13}\text{C}$ showed that the isotopic composition was influenced by atmospheric methane, with a gradient
243 reflecting the transition from source to atmospheric background values (Fig. 2C).



244 To minimize bias from overrepresented datasets in specific regions, our global review consolidated
245 data from each study and region into a single representative value (Fig. 2D and Supplementary
246 Data S2). There appeared to be a significant $\delta^{13}\text{C}$ difference between methane emissions from C3
247 and C4 biomass combustion globally, presumably driven by the differing ^{13}C content of the
248 feedstocks. By weighting $\delta^{13}\text{C}$ values according to the global proportions of C3 and C4 vegetation
249 (77% and 23%) (Still et al., 2003), we derived a global biomass-type-weighted mean $\delta^{13}\text{C}$ value
250 of $-25.0 \pm 2.1\text{‰}$. In contrast, the $\delta^2\text{H}$ values of methane from C3 vs C4 biomass burning did not
251 exhibit a clear distinction (Fig. 2E), suggesting that $\delta^2\text{H}$ was not strongly influenced by biomass
252 type. The mean $\delta^2\text{H}$ value for global biomass burning methane was $-222 \pm 39\text{‰}$.

253 Given that $\delta^{13}\text{C}$ variability in methane from biomass burning was influenced by the relative
254 contributions of C3 and C4 biomass, these factors must be carefully considered when
255 characterizing atmospheric-receptor isotopic signatures in specific regions. Based on our previous
256 isotopic source apportionment of elemental carbon (EC) in South Asian atmospheric aerosols, C3
257 and C4 biomass combustion accounted for 90% and 10% of EC, respectively (Dasari et al., 2020).
258 Since EC and methane are co-emitted during combustion, a first approximation is that they have
259 the same proportional contributions. Using the isotopic values measured for C3 combustion in
260 South Asia, the global mean for C4 combustion, and the regional C3/C4 ratio, we derived a C3/C4-
261 weighted $\delta^{13}\text{C}$ value of $-29.5 \pm 2.0\text{‰}$ for South Asia. In contrast, $\delta^2\text{H}$ was not influenced by C3/C4
262 composition and does not require such adjustment. Overall, methane from biomass burning in
263 South Asia was more depleted in $\delta^{13}\text{C}$ and more enriched in $\delta^2\text{H}$ than the global mean ($-$
264 $25.0 \pm 2.1\text{‰}$).

265 Global wildfire-related methane emissions may be underestimated due to undetected small fires
266 (Zhao et al., 2025), highlighting the need for top-down constraints of biomass burning emissions.



267 Estimate of methane emission from tropical biomass burning spanned a wide range of 14–34 Tg
268 yr^{-1} (Kirschke et al., 2013), making alternative approaches to methane assessments in South Asia
269 particularly important. A recent study reported $\delta^{13}\text{C}$ values of CH_4 from tropical biomass burning,
270 ranging from $-12\text{\textperthousand}$ to $-16\text{\textperthousand}$ for grassland fires and $-16\text{\textperthousand}$ to $-28\text{\textperthousand}$ for farmland fires (Nisbet et
271 al., 2022), which align with global estimates. In tropical regions, the relative proportions of C3
272 and C4 biomass remain a key determinant of isotopic signatures, while geographic variations have
273 a minor influence. Additionally, combustion conditions and fuel moisture content can influence
274 isotopic signatures, necessitating additional research to refine isotopic source characterization
275 (Vernooij et al., 2022).

276 In South Asia, biomass burning is dominated by agricultural residue combustion and other fire
277 types, such as wildfires and forest fires, and are expected to have similar methane isotopic
278 signatures. Other combustion sources, such as traffic and coal combustion, contribute modestly to
279 methane emissions but exhibit $\delta^{13}\text{C}$ signatures of their raw materials similar to C3 biomass (Yao
280 et al., 2022). Improved isotopic characterization of these sources can enhance source attribution.
281 In South Asia, biomass burning emissions displayed more depleted $\delta^{13}\text{C}$ and enriched $\delta^2\text{H}$ values
282 than global means reported from elsewhere, reflecting regional variations in fuel type and C3/C4
283 biomass composition. Region-specific isotopic endmembers are therefore critical for accurate
284 source apportionment.

285

286 **3.2. Methane from ruminants**

287 The isotopic source signatures of ruminant methane from South Asia were constrained and
288 compared with such measurements globally (Fig. 3, Table 2, Supplementary Data S1–S2). The



289 $\delta^{13}\text{C}$ and $\delta^2\text{H}$ values derived from Miller-Tans plots (Fig. 3A–3B), yielded $-68.7\pm0.5\text{\textperthousand}$ (primarily
290 reflecting C3 biomass) and $-343\pm6\text{\textperthousand}$, respectively. Keeling plots yielded comparable $\delta^{13}\text{C}$ and
291 $\delta^2\text{H}$ values (Supplementary Fig. S2). The relationship between $\delta^2\text{H}$ and $\delta^{13}\text{C}$ showed a clear
292 gradient as the isotopic composition transitions from the source to the atmospheric background
293 (Fig. 3C).

294 Methane isotopic values from global ruminant sources were summarized from the literature (Fig.
295 3D), revealing a notable $\delta^{13}\text{C}$ difference between C3 and C4 diets, driven by the distinct ^{13}C
296 content of these feedstocks. By weighting $\delta^{13}\text{C}$ values according to the global proportions of C3
297 and C4 diets (70% and 30%) from a recent database study (Chang et al., 2019), we calculated a
298 global C3/C4 biomass-weighted mean $\delta^{13}\text{C}$ value of $-63.8\pm2.4\text{\textperthousand}$. In contrast, the $\delta^2\text{H}$ values for
299 methane from ruminants globally showed no clear differentiation between C3 and C4 diets (Fig.
300 3E). The global mean $\delta^2\text{H}$ value was $-311\pm46\text{\textperthousand}$, suggesting that $\delta^2\text{H}$ in methane emissions was
301 not strongly influenced by diet composition or rumination processes.

302 Methane emissions from C3-fed ruminants in South Asia ($-68.7\pm0.5\text{\textperthousand}$, Fig. 3A) were more
303 depleted in $\delta^{13}\text{C}$ than the global mean ($-67.0\pm3.0\text{\textperthousand}$, Fig. 3D). However, regional variability in
304 C3/C4 feed composition was an equally important factor that must be considered when
305 determining the representative isotopic signature for South Asian ruminants. Based on a database
306 study (Chang et al., 2019), ruminant diets in South Asia consisted of approximately 65% C3 and
307 35% C4 plants. Using the isotopic values measured for C3 diet ruminants in South Asia, the global
308 mean for C4 diet ruminants, and the regional C3/C4 ratio, we calculated a C3/C4-weighted $\delta^{13}\text{C}$
309 value of $-63.3\pm1.1\text{\textperthousand}$ for South Asia. In contrast, $\delta^2\text{H}$ was not significantly influenced by C3/C4
310 dietary composition and does not require adjustment. After accounting for the C3/C4 feed ratio,
311 the $\delta^{13}\text{C}$ signatures of ruminant methane in South Asia were comparable to the global mean. In



312 contrast, $\delta^2\text{H}$ signatures showed a substantial discrepancy, with depletion exceeding by 32‰ in
313 South Asia compared to the global mean, underscoring the importance of determining and using
314 regionally-constrained source fingerprints in isotope-based source apportionment studies.

315 Recent studies have indicated that biogenic methane emissions have increased in the tropics, with
316 considerable emissions from agricultural activities such as ruminant livestock farming and rice
317 cultivation (Schaefer et al., 2016). South Asia, home to the world's largest ruminant stock, is
318 potentially one of the major contributors to these emissions (Ganesan et al., 2017). Isotopic source
319 fingerprinting to characterize ruminant methane emissions in the tropics and South Asia offers a
320 promising approach to place quantitative constraints on the importance of ruminant and other
321 sources. Isotopic source signatures must be carefully adjusted based on regional dietary
322 compositions and environmental conditions, as the prevalence of C4 vegetation in tropical regions
323 results in more enriched $\delta^{13}\text{C}$ values in some areas, such as $-57\text{\textperthousand}$ in Kenya (Nisbet et al., 2022),
324 -52 to $-57\text{\textperthousand}$ in Zimbabwe (Brownlow et al., 2017), -60 to $-63\text{\textperthousand}$ in Australia (Lu et al., 2021),
325 and $-65\text{\textperthousand}$ in sub-Saharan Africa (Chang et al., 2019). Additionally, methane from ruminants is
326 primarily produced in the rumen through enteric fermentation and then exhaled (Hook et al., 2010),
327 but cattle are not the only ruminants contributing to methane emissions. Other species, such as
328 buffalo, sheep, and goats also play a significant role. Incorporating these additional ruminant
329 sources may help develop a more comprehensive isotopic characterization. Ruminant methane
330 showed similar $\delta^{13}\text{C}$ source signatures globally but displayed distinct $\delta^2\text{H}$ values in South Asia
331 that deviate from the global mean. Taken together, also for the ruminant releases, isotope-based
332 source apportionment of atmospheric methane should employ region-specific endmember values.

333



334 **3.3. Methane from rice paddies**

335 The isotopic signatures of methane from South Asian rice paddies were quantified and compared
336 with global values (Fig. 4, Table 3, Supplementary Data S1–S2). The $\delta^{13}\text{C}$ and $\delta^2\text{H}$ derived from
337 Miller–Tans plots were $-53.8\pm0.8\text{\textperthousand}$ and $-311\pm6\text{\textperthousand}$, respectively (Figs. 4A–B). While Keeling
338 plots exhibited a poor linearity and may be less reliable, they yielded even more enriched $\delta^{13}\text{C}$ and
339 $\delta^2\text{H}$ values (Supplementary Fig. S3). Alternative statistical approaches, quantiles, arithmetic
340 means, and concentration-weighted means, also produced more enriched signatures than the
341 Miller–Tans method (Figs. 4D–E). Among them, the concentration-weighted mean ($\delta^{13}\text{C}=-$
342 $45.3\pm12.3\text{\textperthousand}$, $\delta^2\text{H}=-250\pm71\text{\textperthousand}$) likely reflected methane dissolved in floodwater. A significant
343 linear relationship between $\delta^{13}\text{C}$ and $\delta^2\text{H}$ in rice paddy water (Fig. 4C) was consistent with isotopic
344 enrichment from methane oxidation by methanotrophic bacteria (Schaefer and Whiticar, 2008).
345 However, diffusion through floodwater accounts for only 1–2% of total methane emissions from
346 rice paddies, whereas ~90% is transported via plant-mediated pathways (aerenchyma) and 8–9%
347 through ebullition (Cicerone and Shetter, 1981; Schütz et al., 1989; Smartt et al., 2016). Emissions
348 via plant-mediated transport and ebullition are minimally affected by pre-emission oxidation,
349 while the diffusion pathway is more susceptible to isotopic enrichment through oxidation.
350 Therefore, the Miller–Tans values likely best represented the unoxidized, source-specific isotopic
351 signature of rice paddy methane.

352 The global compilation of $\delta^{13}\text{C}$ and $\delta^2\text{H}$ values of methane emissions from rice paddies and
353 wetlands revealed similar isotopic signatures of these two aqueous sources (Figs. 4F–4G). The
354 global mean $\delta^{13}\text{C}$ and $\delta^2\text{H}$ values for rice paddies were $-59.8\pm5.3\text{\textperthousand}$ and $-324\pm18\text{\textperthousand}$, respectively,
355 while these for wetlands were $-60.0\pm7.6\text{\textperthousand}$ and $-309\pm49\text{\textperthousand}$. Both sources exhibited clear
356 latitudinal trends, with more enriched isotopic signatures in tropical regions and more depleted



357 values in boreal zones. These patterns were consistent with previous observations, which attributed
358 the depletion in boreal wetland $\delta^{13}\text{C}$ to reduced oxidation and the absence of C4 vegetation (France
359 et al., 2022; Brownlow et al., 2017; Tyler et al., 1988; Fisher et al., 2017; Ganesan et al., 2018). In
360 tropical and temperate zones, $\delta^{13}\text{C}$ values for rice paddies and wetlands were nearly identical.
361 However, due to the absence of rice paddies in boreal regions, the global mean $\delta^{13}\text{C}$ value for rice
362 paddy methane appeared slightly more enriched compared to that from wetlands. Conversely,
363 global mean $\delta^2\text{H}$ value was slightly more depleted, potentially reflecting data availability biases,
364 as boreal wetlands exhibited the most depleted $\delta^2\text{H}$ values. Methane from South Asian rice paddies
365 (Miller-Tans values) was notably more enriched in $\delta^{13}\text{C}$ compared to the global mean, while $\delta^2\text{H}$
366 values slightly enriched than global mean. This enrichment was consistent with previous regional
367 measurements (e.g., $\delta^{13}\text{C} = -54.3\text{‰}$ and -57.2‰ ; (Rao et al., 2008)) and might reflect enhanced
368 pre-emission oxidation under South Asian field conditions.

369 Methane formation in rice paddies and wetlands primarily occurs via acetoclastic (acetate
370 fermentation) and hydrogenotrophic (CO_2 reduction with H_2) pathways. The hydrogenotrophic
371 pathway typically yields methane with more depleted $\delta^{13}\text{C}$ values, whereas acetoclastic
372 methanogenesis produces methane with relatively enriched $\delta^{13}\text{C}$ values (Whiticar et al., 1986).
373 The dominant pathway varies with substrate availability, temperature, and redox conditions across
374 wetland and lake types. In wetlands, methane is also emitted through plant-mediated transport
375 (~30%–90%; more than 90% in some studies), ebullition (up to ~60%; more than 90% in non-
376 plant systems), and diffusion (up to ~30%) (Van Der Nat and Middelburg, 1998; Ding et al., 2002;
377 Jeffrey et al., 2019; Villa et al., 2020; Ma et al., 2017), similar to rice paddies but with varying
378 pathway contributions. Both methane source pathways and oxidation processes influence the
379 isotopic composition of these aquatic emissions, although the extent of these effects remains



380 uncertain and requires further study. Given the broad spatial coverage of our dataset, the Miller–
381 Tans values for rice paddy methane reflected minimally oxidized isotopic signatures and were
382 considered regionally representative. In contrast, isotopic values for wetland methane require
383 further evaluation; currently, literature-based values from tropical regions are recommended.
384 Given that approximately half of global methane emissions originate from aquatic ecosystems
385 (Rosentreter et al., 2021) and South Asia accounts for ~20% of global rice production (Ganesan et
386 al., 2017), applying region-specific isotopic source signatures is essential for accurately
387 constraining methane emissions in South Asia.

388

389 **3.4. Methane from wastewater**

390 The isotopic source signatures of methane were constrained from South Asian wastewater and
391 compared with global wastewater sources (Fig. 5, Table 4, Supplementary Data S1–S2). The $\delta^{13}\text{C}$
392 and $\delta^2\text{H}$ values derived from Miller-Tans plots (Figs. 5A–5B), yielded $-46.4\pm1.2\text{\textperthousand}$ and
393 $-355\pm5\text{\textperthousand}$, respectively. Although Keeling plots exhibited poor linearity and may be less reliable,
394 they yielded similar $\delta^{13}\text{C}$ and enriched $\delta^2\text{H}$ values (Supplementary Fig. S4). There was no clear
395 relationship between $\delta^{13}\text{C}$ and $\delta^2\text{H}$ for methane in wastewater (Fig. 5C). The concentration
396 gradient suggested minimal oxidation, indicating that degradation processes prior to release were
397 limited for wastewater methane. The methane isotopic signatures were compared for isotopic
398 quantiles, arithmetic means and concentration-weighted means (Figs 5D–5E). The median- and
399 concentration-weighted means aligned closely with the values obtained from Miller-Tans plots,
400 further supporting their reliability.



401 A global review of $\delta^{13}\text{C}$ and $\delta^2\text{H}$ values was conducted for methane emissions from waste sources
402 (Fig. 5F–5G), i.e., wastewater, landfills and other sources. The results indicated minor differences,
403 suggesting that $\delta^{13}\text{C}$ and $\delta^2\text{H}$ signatures were not significantly distinct among various waste
404 sources. Methane from global waste sources had mean $\delta^{13}\text{C}$ and $\delta^2\text{H}$ values of $-54.0 \pm 5.4\text{‰}$ and $-$
405 $295 \pm 18\text{‰}$, respectively. Slight differences existed between methane emissions from wastewater
406 and landfills, with wastewater showing more enriched $\delta^{13}\text{C}$ and slightly more depleted $\delta^2\text{H}$ values.
407 Other sources, such as composting, biogas fermentation and other organic waste decomposition
408 (Lu et al., 2021; Bakkaloglu et al., 2022), exhibited more dispersed and irregular patterns.
409 Nonetheless, our findings showed that methane isotopic signatures from waste sources were
410 consistent globally, which facilitated isotopic source apportionment. This similarity may be
411 attributed to similar methane production mechanisms across these sources. Additionally, the
412 narrow range of $\delta^{13}\text{C}$ values for global waste methane suggested minimal latitudinal variation,
413 making further differentiation unnecessary. However, in South Asia, methane from wastewater
414 was more enriched in $\delta^{13}\text{C}$ and depleted in $\delta^2\text{H}$ compared to the global mean values.

415 Methane emissions from waste sources were estimated to contribute approximately 12% of global
416 anthropogenic emissions (Saunois et al., 2025). In South Asia, landfill methane emissions were
417 particularly significant (Chakraborty et al., 2011), and atmospheric data also suggested that the
418 waste sector played a key role in regional methane emissions, as supported by $\delta^{13}\text{C}$ constraints
419 (Metya et al., 2022). Emissions from waste sources were also influenced by a range of factors,
420 including microbial communities, temperature, pH, the CH_4/O_2 ratio, nutrient levels and inhibitory
421 chemicals (Polag et al., 2015). Additionally, studies indicated that the operational status of landfills
422 (active or closed) can influence the carbon isotopic signature (Bakkaloglu et al., 2022). However,
423 our global review showed only minor distinctions among various waste sources, suggesting that



424 the isotopic signatures we measured in South Asia should be representative for the region. Further
425 exploring various factors may improve our understanding of methane emissions from the waste
426 sector. Although isotopic signatures of methane from waste sources showed limited variability
427 globally, values in South Asia deviated significantly from the global mean. This highlights the
428 need for region-specific isotopic endmembers also for wastewater in methane source
429 apportionment studies.

430

431 **3.5. Geographical distribution**

432 There are geographic variations in methane isotopic compositions across the globe for any source
433 class due to a combination of environmental factors and source materials. The isotopic signatures
434 of microbial methane vary across regions due to multiple factors, including differences in raw
435 materials, methanogenic pathways (Whiticar et al., 1986; Conrad, 2005), and the methane
436 oxidation by methanotrophic bacteria. These factors are essential to consider and suggests that
437 region-specific and sometimes system-specific isotope source fingerprinting are necessary to
438 facilitate accurate isotope-based source apportionment. Previous studies identified correlations
439 between methane isotopic values and regional environmental factors (Sherwood et al., 2017;
440 Douglas et al., 2021). Building on our isotopic data and a comprehensive literature review, we
441 investigated the geographic distribution of the isotopic signals of microbial methane in South Asia
442 and worldwide.

443 The geographical distribution of methane isotopic signatures in South Asia was assessed for two
444 microbial sources: rice paddies and wastewater (Fig. 6). Regional Miller–Tans-derived values for
445 rice paddy methane showed substantial variability (Fig. 6A), with similar signatures in western



446 India, the Indo-Gangetic Plain (IGP), and Bangladesh, but more depleted values in southern and
447 eastern India. The enrichment in both $\delta^{13}\text{C}$ and $\delta^2\text{H}$ (Fig. 4C) suggested that pre-emission oxidation
448 was the dominant driver of this spatial variation. Given that rice cultivation was concentrated in
449 the IGP and Bangladesh (Gumma, 2011), the production-weighted means of Miller–Tans values
450 ($\delta^{13}\text{C} = -45.5 \pm 2.5\text{‰}$ and $\delta^2\text{H} = -266 \pm 17\text{‰}$) represented pre-oxidation signatures of floodwater
451 methane, though partial oxidation and associated fractionation may still be present. More enriched
452 production-weighted concentration-weighted means ($\delta^{13}\text{C} = -41.7 \pm 7.5\text{‰}$ and $\delta^2\text{H} = -236 \pm 45\text{‰}$)
453 reflected the general oxidation level. Although diffusion contributes only ~1–2% of rice paddy
454 methane emissions, these fractionation patterns may offer insights for wetlands, where diffusion
455 accounts for a larger share (5–30%). Nevertheless, the overall Miller–Tans values ($\delta^{13}\text{C} = -$
456 $53.8 \pm 0.8\text{‰}$ and $\delta^2\text{H} = -311 \pm 6\text{‰}$; Fig. 4A) were minimally influenced by oxidation and best
457 represented the unaltered, source-specific isotopic signature of rice paddy methane.

458 Wastewater methane isotopic signatures exhibited minimal regional variation, with India and
459 Bangladesh showing similar $\delta^{13}\text{C}$ values (Fig. 6B). Pre-emission oxidation of wastewater methane
460 was negligible (Fig. 5C). To better represent regional emissions, we applied population-weighted
461 averaging, assuming similar per capita methane production across areas, yielding $\delta^{13}\text{C} = -$
462 $45.0 \pm 2.4\text{‰}$ and $\delta^2\text{H} = -350 \pm 10\text{‰}$.

463 Our global synthesis revealed pronounced latitudinal variations in the isotopic signatures of
464 methane from wetlands and rice paddies (Figs. 4F–4G). Beyond the effects of oxidation and
465 vegetation type, regional water conditions may also influence the hydrogen isotopic composition
466 of microbial methane. To investigate this, we compared the global distributions of $\delta^2\text{H}$ in surface
467 water (H_2O) and microbial methane (Fig. 7). Surface water isotopic data were sourced from the
468 literature (Nan et al., 2019; Global Network of Isotopes in Precipitation (GNIP); Halder et al.,



469 2015), and microbial methane $\delta^2\text{H}$ values were derived from our dataset and the global review.
470 Global microbial methane $\delta^2\text{H}$ exhibited a moderate correlation with surface water $\delta^2\text{H}$ (Fig. 7),
471 reflecting similar regional patterns. This correlation was particularly pronounced in North America.
472 Hydrogen atoms in surface water likely served as a source for microbial methane, contributing to
473 the observed spatial similarities in isotopic signatures. Among microbial sources, $\delta^2\text{H}$ values
474 varied by source category: ruminants exhibited the most depleted isotopic values, followed by
475 waste, while rice paddies and wetlands were relatively more enriched in isotopic composition. In
476 tropical regions, microbial methane $\delta^2\text{H}$ values were more depleted than global mean values,
477 potentially indicating unique microbial and/or environmental processes that require further
478 investigation. Variations across microbial sources mainly stem from differences in
479 methanogenesis, with each source maintaining internal consistency.

480 Latitudinal variations in aquatic methane $\delta^2\text{H}$ (from rice paddies and wetlands) appeared to be
481 influenced by both water isotopic composition and pre-emission oxidation. In South Asia, $\delta^{13}\text{C}$
482 and $\delta^2\text{H}$ enrichment in rice paddies methane (Fig. 4C) provided clear evidence of oxidation.
483 Additionally, the latitudinal patterns of aquatic methane $\delta^2\text{H}$ closely mirrored those of surface
484 water $\delta^2\text{H}$ (Fig. 7C; Figs. 4F–G), suggesting both factors may contribute. Similarly, ruminant
485 methane exhibited parallel $\delta^2\text{H}$ trends with surface water across latitudes but showed minimal
486 oxidation, as reflected by depleted $\delta^2\text{H}$ values (Fig. 7B) and a narrow $\delta^2\text{H}$ range globally (Fig. 4G),
487 likely due to direct atmospheric release. In contrast, waste sources showed minimal $\delta^2\text{H}$
488 enrichment (Fig. 7D) and narrow $\delta^{13}\text{C}$ and $\delta^2\text{H}$ distributions globally (Figs. 5F–5G), suggesting
489 limited impacts from water sources and oxidation. In comparison, biomass burning methane
490 exhibited a consistently narrow global $\delta^2\text{H}$ range (Fig. 2E), as it was minimally influenced by
491 surface water and was emitted directly into the atmosphere without oxidation.



492 Data scarcity in many regions limited the development of a comprehensive global distribution map
493 (Fig. 7). Some studies supposed that $\delta^2\text{H}$ values provided weaker constraints on methane isotopic
494 sources compared to $\delta^{13}\text{C}$ values (Nisbet et al., 2023), resulting in fewer studies focusing on $\delta^2\text{H}$.
495 Nevertheless, other research indicated correlations between the $\delta^2\text{H}$ of surface water (and
496 precipitation) and the $\delta^2\text{H}$ of aquatic methane sources in certain regions (Douglas et al., 2021). Our
497 results indicated that $\delta^2\text{H}$ followed predictable trends shaped by surface water isotopic composition
498 and microbial processes. The correlation remained valid on a global scale (Fig. 7), though it was
499 weaker, as numerous factors collectively influenced the isotopic signatures of each microbial
500 source. Therefore, incorporating $\delta^2\text{H}$ into isotopic source apportionment can enhance our
501 understanding of the factors driving the rapid rise in global methane concentrations. Despite
502 progress, studies on methane isotopic source signatures remain incomplete, with significant data
503 gaps across many regions. This study alleviated some of these gaps for South Asia, contributing
504 to the required source fingerprint data for isotope-based source apportionment of airshed-receptor
505 methane.

506

507 **4. Summary of methane isotopic signatures in South Asia and globally**

508 The extensive new source-isotope datasets were combined with earlier studies to yield updated
509 dual-isotope endmember databases for South Asia and the globe (Fig. 8 and Table 5). Methane
510 isotopic signatures for several sources differed in South Asia relative to their global means.
511 Biomass burning and ruminant emissions in South Asia, both primarily associated with C3
512 biomass, exhibited more depleted $\delta^{13}\text{C}$ values than global means (Fig. 8A). Conversely, methane
513 from rice paddies and wastewater displayed more enriched $\delta^{13}\text{C}$ values than global means. For
514 $\delta^2\text{H}$, methane from biomass burning and thermogenic sources in South Asia was more enriched



515 than global means (Fig. 8B). Among microbial sources, ruminants and wastewater were more
516 depleted in $\delta^2\text{H}$, while rice paddies were more enriched than global values. The $\delta^2\text{H}$ versus $\delta^{13}\text{C}$
517 comparisons between South Asian and global methane sources provided a two-dimensional
518 perspective (Fig. 9). While South Asian sources generally aligned with global categories, they
519 exhibited distinct deviations. South Asian isotopic signatures showed a narrower distribution,
520 whereas global isotopic signatures displayed greater variability. Among microbial sources, South
521 Asian isotopic signatures appeared tighter constrained than their global counterparts.

522 Based on previous bottom-up and top-down studies, emissions-weighted microbial methane
523 isotopic signatures in South Asia ranged from $\delta^{13}\text{C} = -54.6 \pm 1.2\text{\textperthousand}$ and $\delta^2\text{H} = -323 \pm 8\text{\textperthousand}$ (Ito et al.,
524 2023) to $\delta^{13}\text{C} = -57.1 \pm 1.8\text{\textperthousand}$ and $\delta^2\text{H} = -329 \pm 11\text{\textperthousand}$ (Saunois et al., 2025). These $\delta^{13}\text{C}$ values are
525 notably more enriched than the global compiled one ($\delta^{13}\text{C} = -60.2 \pm 4.8$ and $\delta^2\text{H} = -308 \pm 32$)
526 (Masson-Delmotte et al., 2021; Saunois et al., 2025), largely due to substantial rice paddy and
527 waste contributions. Considering the $\delta^{13}\text{C}$ of atmospheric methane in South Asia (e.g.,
528 $-47.41 \pm 0.94\text{\textperthousand}$ in India (Metya et al., 2022)) and accounting for isotopic fractionation during OH
529 oxidation (approximately 6–7‰ in $\delta^{13}\text{C}$ (Whiticar and Schaefer, 2007; Fischer et al., 2008;
530 Schwietzke et al., 2016)), the inferred isotopic values of the total source approach or even fall
531 below the microbial estimates. This discrepancy suggests biases in current emission inventories,
532 likely overestimating rice paddy emissions and underrepresenting other microbial sources. These
533 uncertainties highlight the need for dual-isotope measurements at receptor sites to better constrain
534 methane budgets in South Asia.

535



536 **5. Concluding discussion**

537 Methane emission estimates remain considerably uncertain. Some studies attributed recent
538 atmospheric methane increases primarily to microbial sources, including tropical wetlands
539 (Saunois et al., 2025), waste and agriculture (Peng et al., 2022; Michel et al., 2024), while others
540 highlighted contributions from thermogenic and ruminant sources (Chandra et al., 2021). Biomass
541 burning was also proposed as a significant contributor (Zhao et al., 2025). Bottom-up inventories
542 showed large discrepancies, with estimates differing by severalfold (Stavert et al., 2022). In South
543 Asia, reported emissions varied substantially in both magnitude and source composition, from
544 $37 \pm 3.7 \text{ Tg C yr}^{-1}$ in the 2000s (Patra et al., 2013) to more recent values of $50.3 \text{ Tg C yr}^{-1}$ (Ito et
545 al., 2023), and 52 Tg C yr^{-1} for top-down (n=6) and 58 Tg C yr^{-1} for bottom-up (n=27) (Saunois
546 et al., 2025). Methane emissions in South Asia exhibited pronounced seasonal variations in both
547 mixing ratios and isotopic composition (Rao et al., 2008; Tiwari et al., 2020; Metya et al., 2022;
548 Guha et al., 2018), reflecting dynamic shifts in source activity that are difficult to capture using
549 conventional models. Given these uncertainties, dual-isotope top-down approaches offer an
550 independent and valuable tool for constraining regional methane budgets.

551 Comparisons of methane isotopic signatures between South Asian and global means revealed
552 significant distinction (Figs. 8–9), underscoring the need for region-specific isotopic data to ensure
553 accurate source apportionment. $\delta^{13}\text{C}$ signatures reflected feedstock characteristics, distinguishing
554 sources such as biomass burning and ruminants based on C3/C4 biomass ratios. Similarly, aquatic
555 methane $\delta^{13}\text{C}$ was influenced by organic precursors, with South Asian sources showing enriched
556 values compared to other regions. Globally, $\delta^2\text{H}$ in methane appeared linked to surface water and
557 organic interactions, but highly depleted $\delta^2\text{H}$ observed in South Asia suggests different microbial
558 processes requiring further investigation. Additionally, pre-emission oxidation significantly

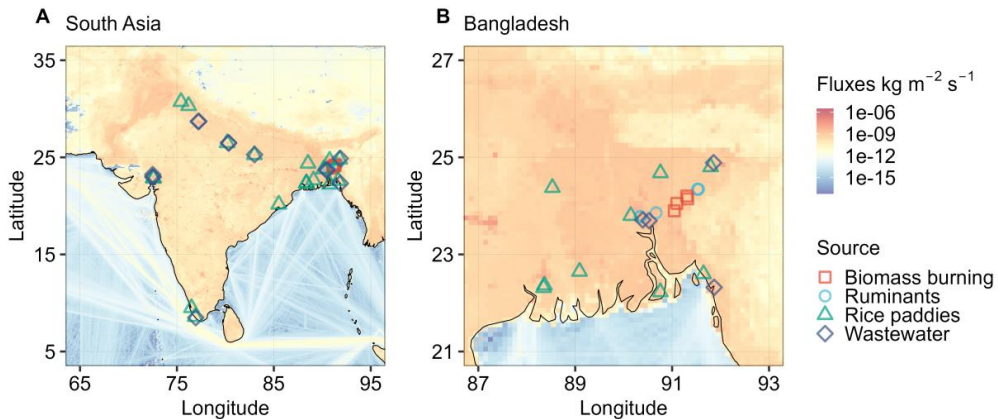


559 affected methane from rice paddy water in South Asia, warranting more research to better
560 understand this process and similar processes in other aqueous sources.

561 The availability and accuracy of isotopic source signatures was critical for constraining methane
562 sources (Schwietzke et al., 2016). At present, isotopic measurements of tropical methane sources
563 remain scarce, particularly for $\delta^2\text{H}$, still limiting their use in atmospheric top-down source
564 constraints. While $\delta^{13}\text{C}$ -based constraints are growing in applications globally (Nisbet et al., 2023),
565 $\delta^2\text{H}$ constraints have been underutilized due to data limitations and unclear geographical
566 distribution. Our study enhances the isotopic source fingerprint database, especially by adding $\delta^2\text{H}$
567 data for sources in South Asia.

568 While isotopic source signatures of major methane sources in South Asia are now improved,
569 estimating the isotopic composition of well-mixed atmospheric methane remains challenging due
570 to potential fractionation during oxidation (e.g., OH and Cl radicals). Existing models applied fixed
571 isotopic fractionation factors, yet these vary considerably across studies (Whiticar and Schaefer,
572 2007; Fischer et al., 2008; Rice et al., 2016; Schwietzke et al., 2016; Schaefer et al., 2016; Bock
573 et al., 2017; Sherwood et al., 2017; Douglas et al., 2021; Nisbet et al., 2023; Michel et al., 2024;
574 Thanwerdas et al., 2024; Fujita et al., 2025). Despite these uncertainties, background methane
575 mixing ratios and isotopic compositions in South Asia and globally remain relatively stable,
576 indicating that a steady-state approach, incorporating region-specific isotopic fingerprints, may
577 help reconcile inconsistencies in current methane budget estimates.

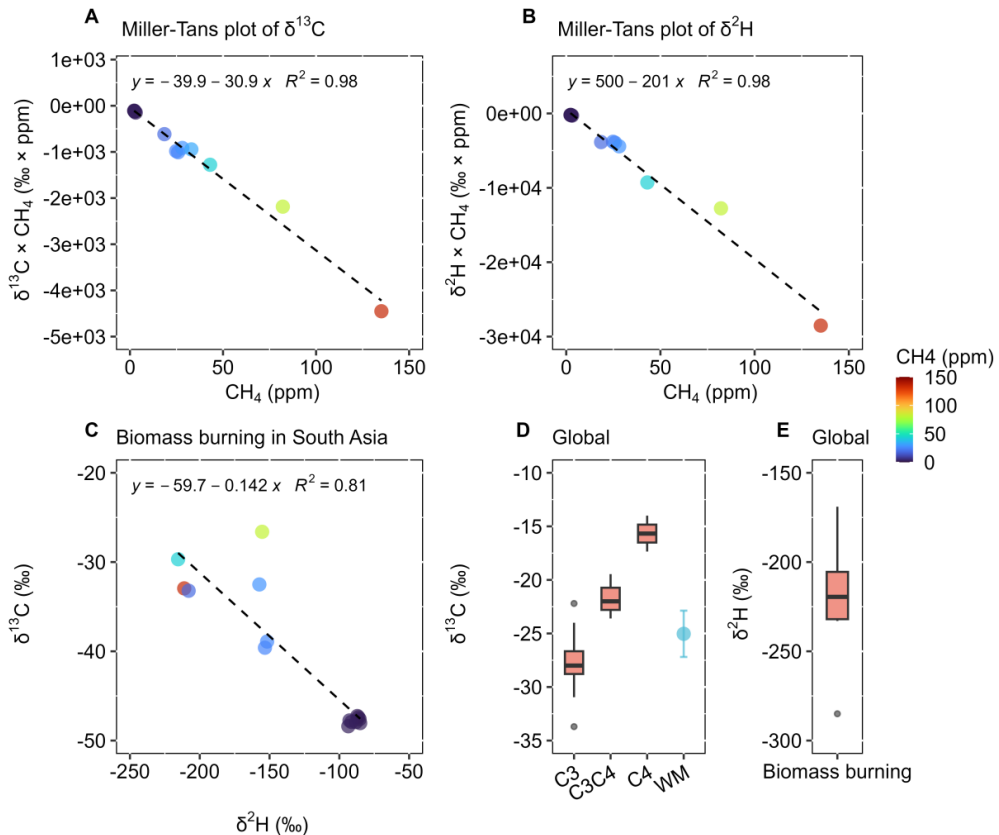
578



579

580 **Fig. 1. Map of collected methane source samples for (A) entire South Asia and (B) a close-up**
581 **for Bangladesh.** The background color represents total methane fluxes in 2023, sourced from
582 EDGAR (Crippa et al., 2021).

583



584

585 **Fig. 2. Isotopic characteristics of methane from biomass burning in South Asia and globally.**

586 (A) Miller-Tans plot of $\delta^{13}\text{C}$ -CH₄ for South Asia crop residue burning. (B) Miller-Tans plot of
 587 $\delta^2\text{H}$ -CH₄ for South Asia crop residue burning. (C) Coupled variation in $\delta^{13}\text{C}$ and $\delta^2\text{H}$. (D) Global
 588 $\delta^{13}\text{C}$ values of biomass burning methane (C3 vs. C4 biomass, WM=weighted mean of C3 and C4
 589 biomass). (E) Global $\delta^2\text{H}$ values of biomass burning methane. Biomass burning in South Asia
 590 primarily here refer to agricultural wheat crop residue burning. Global review in Supplementary
 591 Data S2.

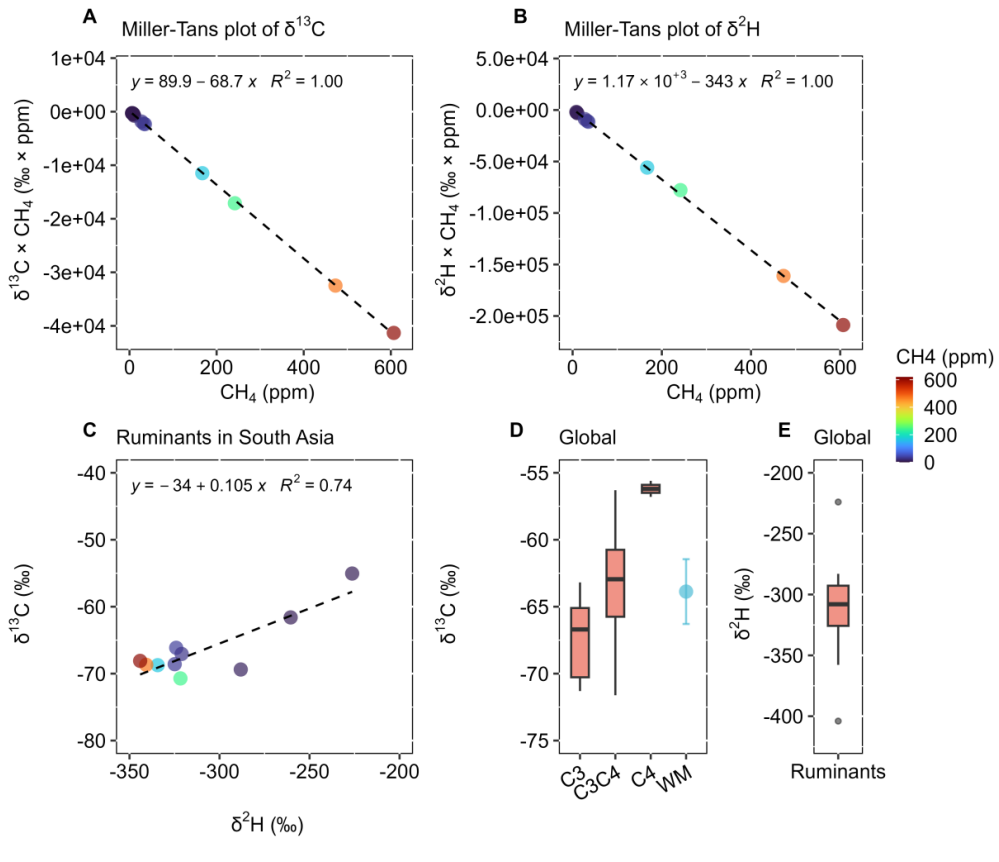
592



593 **Table 1. Isotopic signatures of CH₄ from biomass burning in South Asia and globally, as**
594 **determined by various analytical and statistical methods.**

	Region	Type	$\delta^{13}\text{C}$ (‰)	$\delta^2\text{H}$ (‰)	Data/Ref.
Keeling Miller-Tans	South Asia	C3	-31.6 ± 2.7	-186 ± 19	Data S1
	South Asia	C3	-30.9 ± 2.2	-201 ± 18	Data S1
	South Asia	WM of C3/C4*	-29.5 ± 2.0		Data S1
Review	Global	C3	-27.8 ± 2.7		Data S2
	Global	C4	-15.7 ± 2.4		Data S2
	Global	C3&C4	-21.7 ± 2.1		Data S2
	Global	WM of C3/C4	-25.0 ± 2.2		Data S2
	Global	Mean		-222 ± 39	Data S2

595 *The weighted mean (WM) δ -values for biomass burning methane in South Asia are based on a
596 C3:C4 ratio of 0.9:0.1, derived from an EC isotopic source apportionment study (Dasari et al.,
597 2020). For the global biomass burning methane, the WM is calculated using a C3:C4 ratio of
598 0.77:0.23, based on the global distribution of C3 and C4 vegetation (Still et al., 2003).



601 **Fig. 3. Isotopic characteristics of methane from ruminants in South Asia and globally. (A)**
 602 Miller-Tans plot of $\delta^{13}\text{C}$ -CH₄ for South Asia ruminants. (B) Miller-Tans plot of $\delta^2\text{H}$ -CH₄ for South
 603 Asia ruminants. (C) Coupled variation in $\delta^{13}\text{C}$ and $\delta^2\text{H}$. (D) Global $\delta^{13}\text{C}$ values of ruminant
 604 methane (C3 vs. C4 diets; WM=weighted mean of C3 and C4 diets). (E) Global $\delta^2\text{H}$ values of
 605 ruminant methane. Global review in Supplementary Data S2.

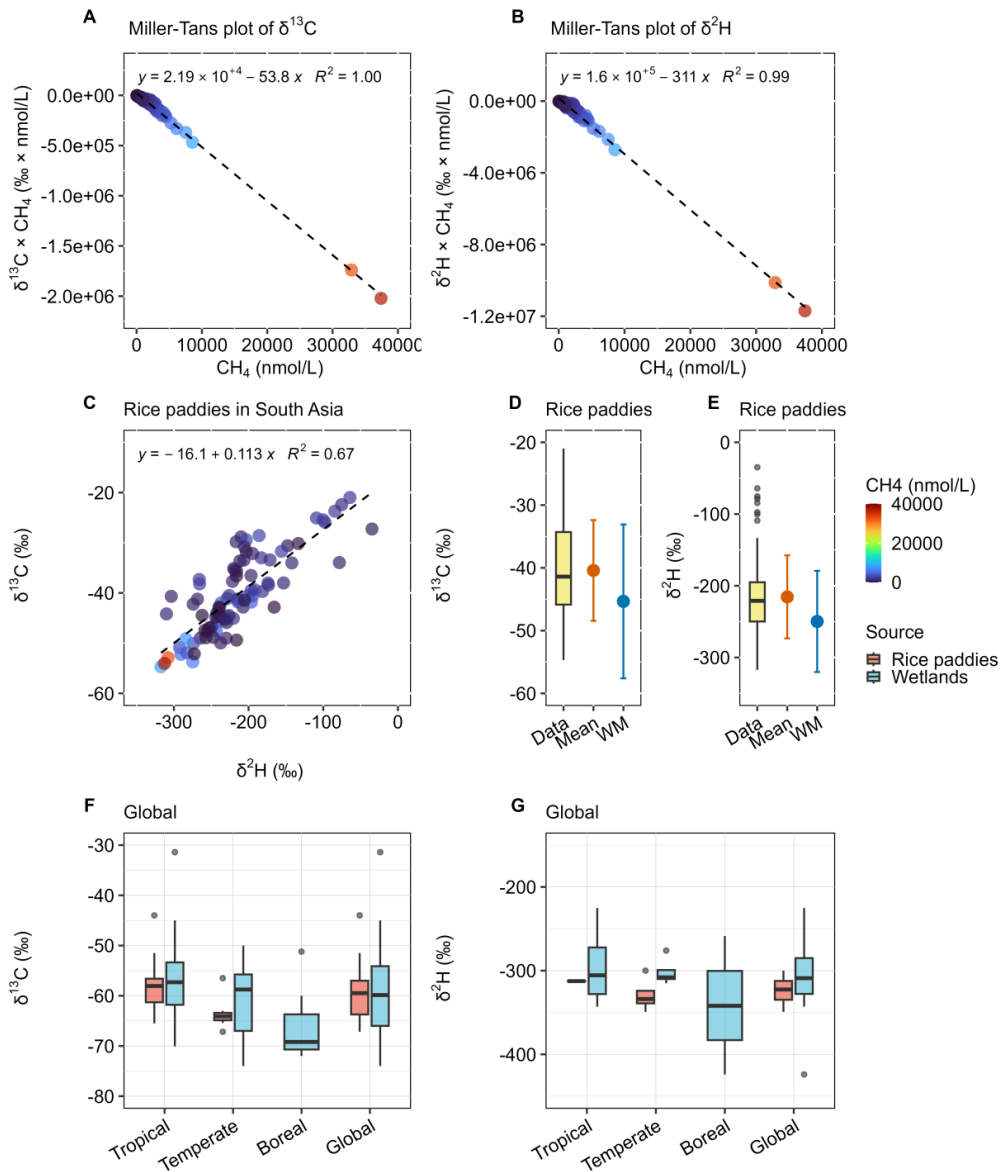
606



607 **Table 2. Isotopic signatures of CH₄ from ruminants in South Asia and globally, as**
608 **determined by various analytical and statistical methods.**

	Region	Type	$\delta^{13}\text{C}$ (‰)	$\delta^2\text{H}$ (‰)	Data/Ref.
Keeling Miller-Tans	South Asia	C3	-71.0±3.8	-342±13	Data S1
	South Asia	C3	-68.7±0.5	-343±6	Data S1
	South Asia	WM of C3/C4*	-63.3±1.1		Data S1
Review	Global	C3	-67.0±3.0		Data S2
	Global	C4	-53.2±3.1		Data S2
	Global	C3&C4	-61.3±6.4		Data S2
	Global	WM of C3/C4	-63.8±2.4		Data S2
	Global	Mean		-311±46	Data S2

609 *The weighted mean (WM) δ -values for ruminant methane in South Asia are based on a C3:C4
610 dietary of 0.65:0.35, reflecting the regional distribution of ruminant feed (Chang et al., 2019). For
611 the global ruminant methane, the WM is calculated using a C3:C4 ratio of 0.7:0.3, based on the
612 global mean feed composition (Chang et al., 2019).



614

615 **Fig. 4. Isotopic characteristics of methane from rice paddies South Asia and globally. (A)**
 616 Miller-Tans plot of $\delta^{13}\text{C-CH}_4$ for South Asia rice paddies. **(B)** Miller-Tans plot of $\delta^2\text{H-CH}_4$ for
 617 South Asia rice paddies. **(C)** Coupled variation in $\delta^{13}\text{C}$ and $\delta^2\text{H}$. **(D)** Quantiles, arithmetic mean,
 618 and concentration-weighted mean of $\delta^{13}\text{C-CH}_4$ for South Asia rice paddies. **(E)** Quantiles,



619 arithmetic mean, and concentration-weighted mean of $\delta^2\text{H-CH}_4$ for South Asia rice paddies. (F)

620 Global $\delta^{13}\text{C}$ values of methane from rice paddies and for comparison also from wetlands. (G)

621 Global $\delta^2\text{H}$ values of methane from rice paddies and for comparison also from wetlands. Global

622 review in Supplementary Data S2.

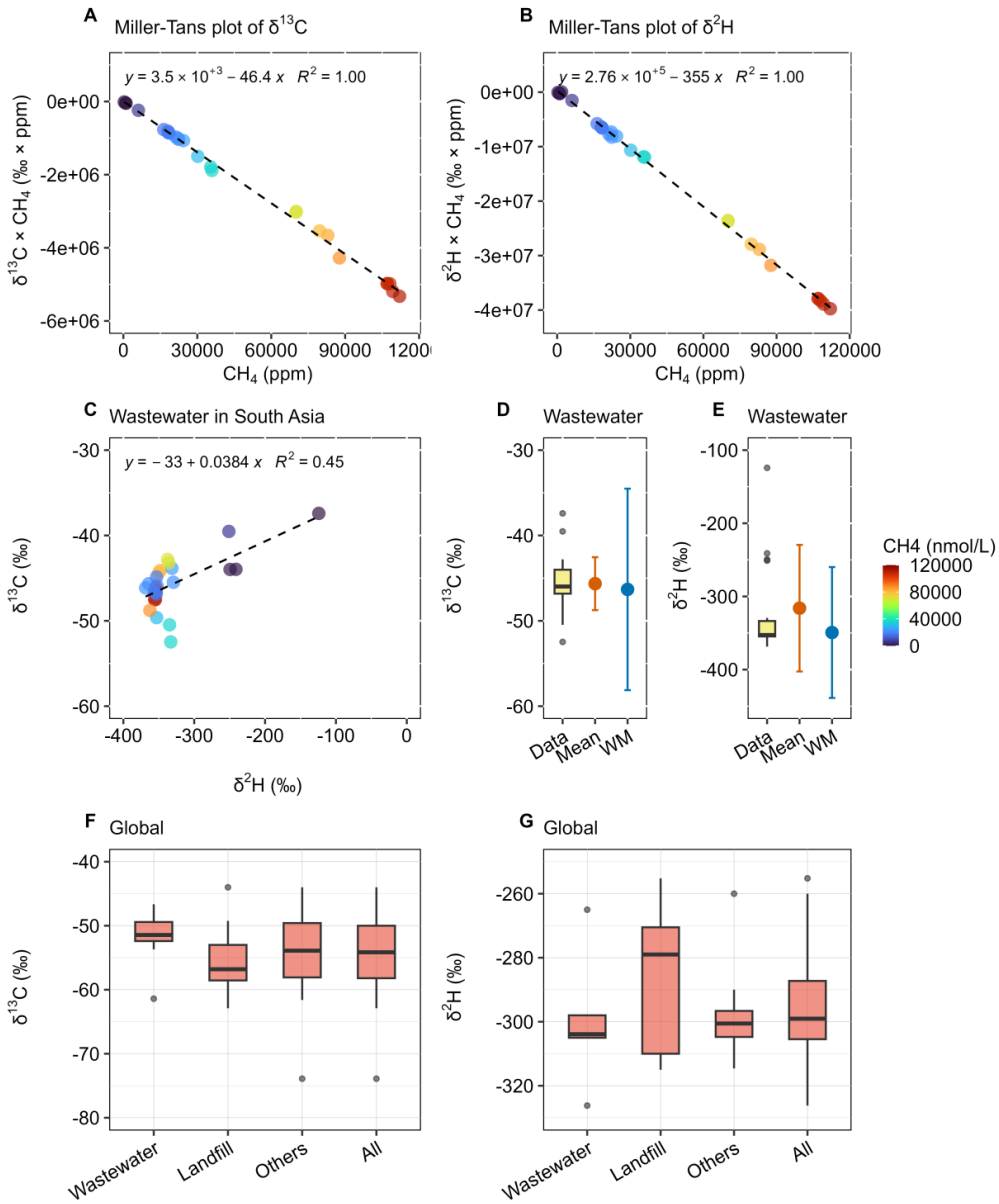
623



624 **Table 3. Isotopic signatures of CH₄ from rice paddies and wetlands in South Asia and**
625 **globally, as determined by various analytical and statistical methods.**

	Region	Type	$\delta^{13}\text{C}$ (‰)	$\delta^2\text{H}$ (‰)	Data/Ref.
Keeling	South Asia		-39.7±1.7	-212±14	Data S1
Miller-Tans	South Asia		-53.8±0.8	-311±6	Data S1
Data analysis	South Asia	Median	-41.4	-221	Data S1
<i>Rice paddies</i>	South Asia	Mean	-40.4±8.0	-215±58	Data S1
	South Asia	WM of conc*	-45.3±12.3	-250±71	Data S1
	South Asia	WM of geo conc	-41.7±7.5	-236±45	Data S1
	South Asia	WM of geo MT	-45.5±2.5	-266±17	Data S1
Review	Global	Mean	-59.8±5.3	-324±18	Data S2
<i>Rice paddies</i>	Tropical	Mean	-58.0±5.2	-313±1	Data S2
	Temperate	Mean	-63.5±3.4	-329±21	Data S2
Review	Global	Mean	-60.0±7.6	-309±49	Data S2
<i>Wetlands</i>	Tropical	Mean	-57.1±7.0	-295±52	Data S2
	Temperate	Mean	-60.5±6.9	-302±15	Data S2
	Boreal	Mean	-66.6±5.4	-342±83	Data S2
Review	Global	Mean	-60.0±7.2	-314±42	Data S2
<i>All</i>	Tropical	Mean	-57.3±6.6 (m=47)	-301±41 (m=4)	Data S2
	Temperate	Mean	-61.1±6.4	-314±22	Data S2
	Boreal	Mean	-66.6±5.4	-342±83	Data S2

626 *“WM of conc” refers to the concentration-weighted mean δ -values of rice paddy methane in
627 South Asia. “WM of geo conc” represents the geographically weighted mean, where each region's
628 contribution is based on its concentration-weighted mean. “WM of geo MT” denotes the
629 geographically weighted mean derived from Miller-Tans method results for each region.



631

632 **Fig. 5. Isotopic characteristics of methane from South Asian wastewater and global waste**
 633 **sources.** **(A)** Miller-Tans plot of $\delta^{13}\text{C}$ -CH4 for South Asia wastewater. **(B)** Miller-Tans plot of
 634 $\delta^2\text{H}$ -CH4 for South Asia wastewater. **(C)** Coupled variation in $\delta^{13}\text{C}$ and $\delta^2\text{H}$. **(D)** Quantiles,



635 arithmetic mean, and concentration-weighted mean of $\delta^{13}\text{C-CH}_4$ for South Asia wastewater. **(E)**
636 Quantiles, arithmetic mean, and concentration-weighted mean of $\delta^2\text{H-CH}_4$ for South Asia
637 wastewater. **(F)** Global $\delta^{13}\text{C}$ values of methane from waste sources. **(G)** Global $\delta^2\text{H}$ values of
638 methane from waste sources. Global review in Supplementary Data S2.

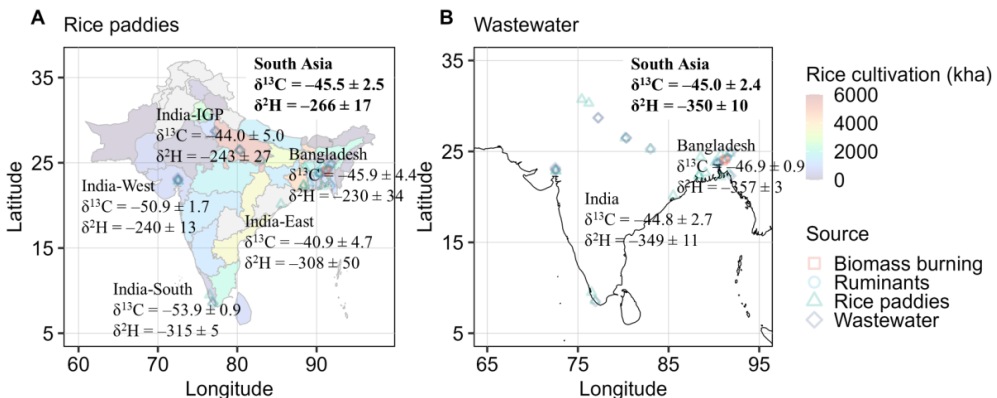
639



640 **Table 4. Isotopic signatures of CH₄ from waste sources in South Asia and globally, as**
641 **determined by various analytical and statistical methods.**

	Region	Type	$\delta^{13}\text{C}$ (‰)	$\delta^2\text{H}$ (‰)	Data/Ref.
Keeling	South Asia	C3	-46.3±1.1	-338±29	Data S1
Miller-Tans	South Asia	C3	-46.4±1.2	-355±5	Data S1
Data analysis	South Asia	Median	-46.0	-353	Data S1
<i>Wastewater</i>	South Asia	Mean	-45.6±3.1	-316±87	Data S1
	South Asia	WM of conc*	-46.3±11.8	-349±89	Data S1
	South Asia	WM of pop MT	-45.0±2.4	-350±10	Data S1
Review	Global	Mean	-54.0±5.4	-295±18	Data S2
	Wastewater	Mean	-51.5±3.8	-300±22	Data S2
	Landfills	Mean	-55.7±4.3	-286±22	Data S2
	Others	Mean	-53.7±6.3	-299±13	Data S2

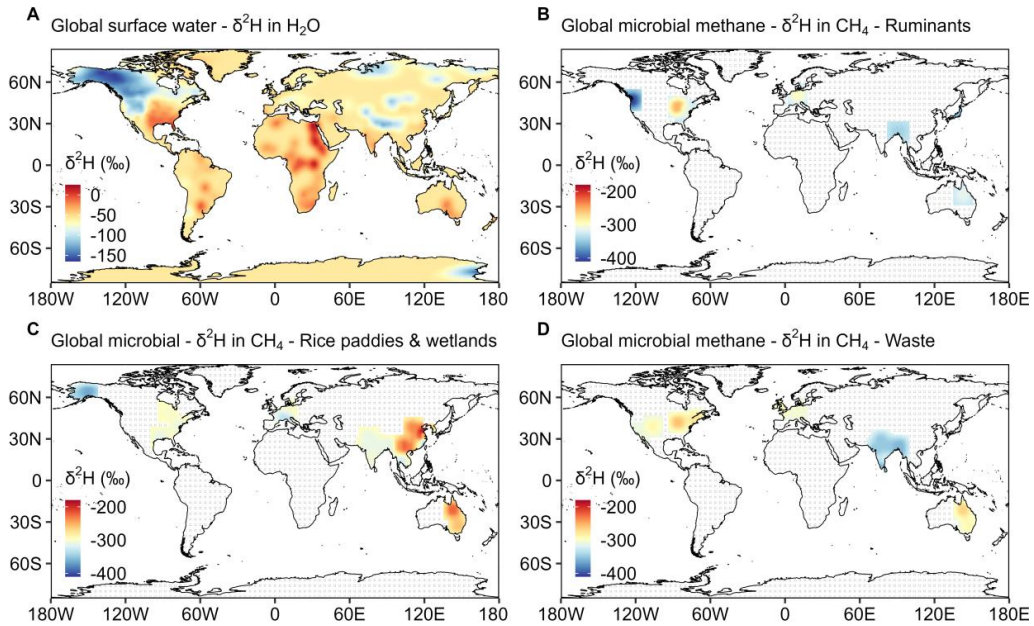
642 *“WM of conc” refers to the concentration-weighted mean δ -values of wastewater methane in
643 South Asia. “WM of pop MT” denotes the population-weighted mean (weighted with the
644 population of each province), calculated from the Miller-Tans method results for each region.



646

647 **Fig. 6. Geographical distribution of methane isotopic signatures from two microbial sources**
648 **in South Asia. (A) Rice paddies. (B) Wastewater.** Rice cultivation data is derived from MODIS
649 multitemporal data (Gumma, 2011). The isotopic signatures for rice paddies represent cultivation-
650 weighted means, while those for wastewater are population-weighted means.

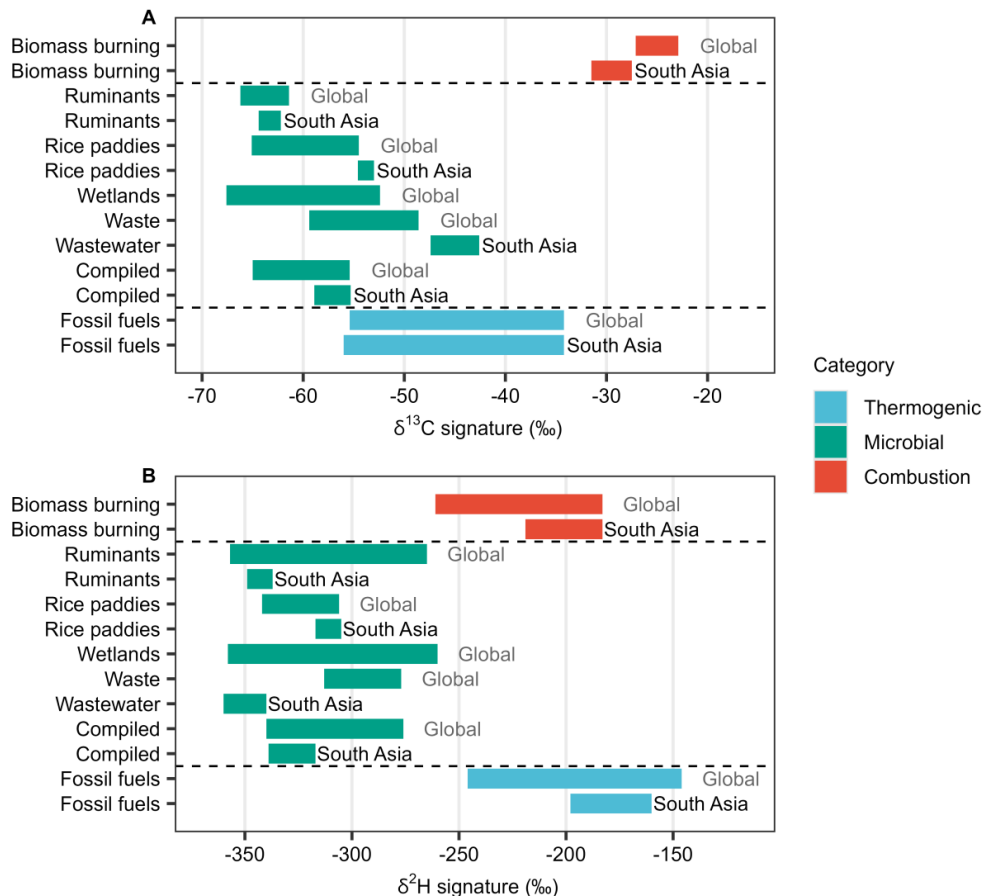
651



652

653 **Fig. 7. Global distribution of $\delta^2\text{H}$ in surface water and in microbial methane.** (A) $\delta^2\text{H}$
654 distribution in surface water systems, based on isotopic data from the literature (Nan et al., 2019;
655 Global Network of Isotopes in Precipitation (GNIP); Halder et al., 2015). (B) $\delta^2\text{H}$ distribution in
656 microbial methane from ruminants. (C) $\delta^2\text{H}$ distribution in microbial methane from rice paddies
657 and wetlands. (D) $\delta^2\text{H}$ distribution in microbial methane from waste. The isotopic and geographic
658 data of microbial methane are compiled from this study (South Asia) and the literature - global
659 (Sherwood et al., 2017) and European (Menoud et al., 2022). Grid cells without any observation
660 are marked with diagonal lines to indicate interpolation-only areas.

661



662

663 **Fig. 8. Isotopic signatures of major methane sources in South Asia and globally. (A) $\delta^{13}\text{C}$**

664 **signatures. (B) $\delta^2\text{H}$ signatures.**

665

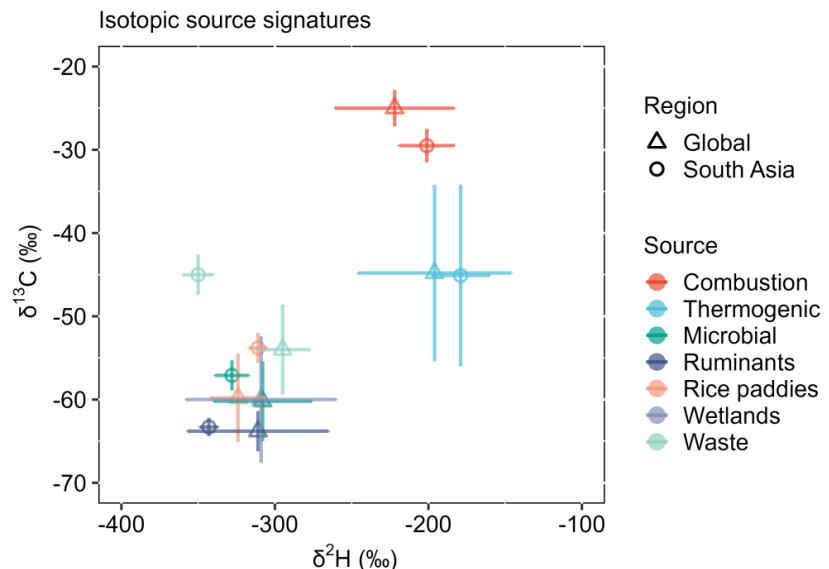


666 **Table. 5. Isotopic signatures of major methane sources in South Asia and globally. n**
667 represents to the number of samples analyzed in this study, while **m** indicates the number of
668 literature sources summarized, where isotopic data from a specific region in a single study are
669 compiled as a single entry. **x** refers to the number of isotopic data from the literature. Raw data,
670 literature review and corresponding references are provided in Supplementary Data S1–S2.

Category	Source	Region	$\delta^{13}\text{C}$ (‰)	$\delta^2\text{H}$ (‰)
Combustion	Biomass burning	South Asia	-30.9 ± 2.2 (n=17; 100% C3) -29.5 ± 2.0 (90% C3)	-201 ± 18 (n=15)
	Biomass burning	Global	-25.0 ± 2.2 (m=19; 77% C3)	-222 ± 39 (m=6)
Microbial	Ruminants	South Asia	-68.7 ± 0.5 (n=37; 100% C3) -63.3 ± 1.1 (65% C3)	-343 ± 6 (n=11)
	Ruminants	Global	-63.8 ± 2.4 (m=36; 70% C3)	-311 ± 46 (m=11)
	Rice paddies	South Asia	-53.8 ± 0.8 (n=90)	-311 ± 6 (n=90)
	Rice paddies	Global	-59.8 ± 5.3 (m=20)	-324 ± 18 (m=6)
	Wetlands	Tropical	-57.3 ± 6.6 (m=47)	-301 ± 41 (m=4)
	Wetlands	Global	-60.0 ± 7.6 (m=94)	-309 ± 49 (m=12)
	Wastewater	South Asia	-45.0 ± 2.4 (n=27)	-350 ± 10 (n=27)
	Waste	Global	-54.0 ± 5.4 (m=69)	-295 ± 18 (m=29)
	Compiled	South Asia	-57.1 ± 1.8	-328 ± 11
	Compiled	Global	-60.2 ± 4.8	-308 ± 32
Thermogenic (mainly)	Fossil fuels	South Asia	-45.1 ± 10.9 (x=83)	-179 ± 19 (x=28)
	Fossil fuels	Global	-44.8 ± 10.6 (x=8128)	-196 ± 50 (x=2878)

671

672



673

674 **Fig. 9. Comparison of South Asian and global isotopic signatures of methane sources.** $\delta^2\text{H}$
675 versus $\delta^{13}\text{C}$. Microbial source refers to the compiled values of ruminants, rice paddies, wetlands,
676 waste, etc.

677



678 **Data availability**

679 The dataset will be hosted and maintained by a database management at the Bolin Centre for
680 Climate Research at Stockholm University. The dataset is accessible at the Bolin Centre Database
681 (<https://bolin.su.se/data/draft?id=14278&token=f0770bfd-210f-4a51-a9bd-a355467058a4>).

682

683 **Supporting Information**

684 Supporting Information for this study is available.

685

686 **Author Contribution**

687 ÖG acquired funding and conceived the study. ÖG, HH, A. Salam, K. Budhavant, MRM, KSJ,
688 MAH, A. Singh, AP, NR, CM, KR, and GKS. designed and conducted the field campaigns. PY,
689 K. Belec, JB, and HH performed the isotope analyses. PY, K. Belec, HH, and ÖG conducted the
690 data analysis and interpretation. PY, HH, and ÖG prepared the manuscript with contributions from
691 all co-authors. All authors reviewed and edited the manuscript.

692

693 **Competing interests**

694 The authors declare that they have no conflict of interest.

695



696 **Acknowledgements**

697 We thank Dr. Fangping Yan, Dr. Joakim Romson, Ms. Marenka Brussee, and Mr. Albin Eriksson
698 for their insightful discussions. This work was supported by the Swedish Research Council VR
699 (Distinguished Professor Grant No. 2017-01601) and the Swedish Research Council for
700 Sustainable Development Formas (Grant No. 2023-01234).

701



702 **References**

703 Bakkaloglu, S., Lowry, D., Fisher, R. E., Menoud, M., Lanoiselé, M., Chen, H., Röckmann, T.,
704 and Nisbet, E. G.: Stable isotopic signatures of methane from waste sources through atmospheric
705 measurements, *Atmos. Environ.*, 276, 119021, <https://doi.org/10.1016/j.atmosenv.2022.119021>,
706 2022.

707 Bock, M., Schmitt, J., Beck, J., Seth, B., Chappellaz, J., and Fischer, H.: Glacial/interglacial
708 wetland, biomass burning, and geologic methane emissions constrained by dual stable isotopic
709 CH₄ ice core records, *Proc. Natl. Acad. Sci.*, 114, E5778–E5786,
710 <https://doi.org/10.1073/pnas.1613883114>, 2017.

711 Bousquet, P., Ciais, P., Miller, J. B., Dlugokencky, E. J., Hauglustaine, D. A., Prigent, C., Van der
712 Werf, G. R., Peylin, P., Brunke, E.-G., Carouge, C., Langenfelds, R. L., Lathière, J., Papa, F.,
713 Ramonet, M., Schmidt, M., Steele, L. P., Tyler, S. C., and White, J.: Contribution of anthropogenic
714 and natural sources to atmospheric methane variability, *Nature*, 443, 439–443,
715 <https://doi.org/10.1038/nature05132>, 2006.

716 Brownlow, R., Lowry, D., Fisher, R. E., France, J. L., Lanoiselé, M., White, B., Wooster, M. J.,
717 Zhang, T., and Nisbet, E. G.: Isotopic Ratios of Tropical Methane Emissions by Atmospheric
718 Measurement, *Global Biogeochem. Cycles*, 31, 1408–1419,
719 <https://doi.org/10.1002/2017GB005689>, 2017.

720 Chakraborty, M., Sharma, C., Pandey, J., Singh, N., and Gupta, P. K.: Methane emission
721 estimation from landfills in Delhi: A comparative assessment of different methodologies, *Atmos.*
722 *Environ.*, 45, 7135–7142, <https://doi.org/10.1016/j.atmosenv.2011.09.015>, 2011.



723 Chandra, N., Patra, P. K., Bisht, J. S. H., Ito, A., Umezawa, T., Saigusa, N., Morimoto, S., Aoki,
724 S., Janssens-Maenhout, G., Fujita, R., Takigawa, M., Watanabe, S., Saitoh, N., and Canadell, J.
725 G.: Emissions from the Oil and Gas Sectors, Coal Mining and Ruminant Farming Drive Methane
726 Growth over the Past Three Decades, *J. Meteorol. Soc. Japan. Ser. II*, 99, 2021–015,
727 <https://doi.org/10.2151/jmsj.2021-015>, 2021.

728 Chang, J., Peng, S., Ciais, P., Saunois, M., Dangal, S. R. S., Herrero, M., Havlík, P., Tian, H., and
729 Bousquet, P.: Revisiting enteric methane emissions from domestic ruminants and their $\delta^{13}\text{CCH}_4$
730 source signature, *Nat. Commun.*, 10, 3420, <https://doi.org/10.1038/s41467-019-11066-3>, 2019.

731 Cicerone, R. J. and Shetter, J. D.: Sources of atmospheric methane: Measurements in rice paddies
732 and a discussion, *J. Geophys. Res. Ocean.*, 86, 7203–7209,
733 <https://doi.org/10.1029/JC086iC08p07203>, 1981.

734 Conrad, R.: Quantification of methanogenic pathways using stable carbon isotopic signatures: a
735 review and a proposal, *Org. Geochem.*, 36, 739–752,
736 <https://doi.org/10.1016/j.orggeochem.2004.09.006>, 2005.

737 Crippa, M., Guzzardi, D., Solazzo, E., Muntean, M., Schaaf, E., Monforti-Ferrario, F., Banja, M.,
738 Olivier, J., Grassi, G., and Rossi, S.: GHG emissions of all world countries, *Publ. Off. Eur. Union*,
739 2021.

740 Cusworth, D. H., Duren, R. M., Ayasse, A. K., Jiorle, R., Howell, K., Aubrey, A., Green, R. O.,
741 Eastwood, M. L., Chapman, J. W., Thorpe, A. K., Heckler, J., Asner, G. P., Smith, M. L., Thoma,
742 E., Krause, M. J., Heins, D., and Thorneloe, S.: Quantifying methane emissions from United States
743 landfills, *Science* (80-), 383, 1499–1504, <https://doi.org/10.1126/science.adl7735>, 2024.



744 Dasari, S., Andersson, A., Stohl, A., Evangelou, N., Bikkina, S., Holmstrand, H., Budhavant, K.,
745 Salam, A., and Gustafsson, Ö.: Source Quantification of South Asian Black Carbon Aerosols with
746 Isotopes and Modeling, Environ. Sci. Technol., 54, 11771–11779,
747 <https://doi.org/10.1021/acs.est.0c02193>, 2020.

748 Ding, W., Cai, Z., Tsuruta, H., and Li, X.: Effect of standing water depth on methane emissions
749 from freshwater marshes in northeast China, Atmos. Environ., 36, 5149–5157,
750 [https://doi.org/10.1016/S1352-2310\(02\)00647-7](https://doi.org/10.1016/S1352-2310(02)00647-7), 2002.

751 Douglas, P. M. J., Stratigopoulos, E., Park, S., and Phan, D.: Geographic variability in freshwater
752 methane hydrogen isotope ratios and its implications for global isotopic source signatures,
753 Biogeosciences, 18, 3505–3527, <https://doi.org/10.5194/bg-18-3505-2021>, 2021.

754 Dyonisius, M. N., Petrenko, V. V., Smith, A. M., Hua, Q., Yang, B., Schmitt, J., Beck, J., Seth,
755 B., Bock, M., Hmiel, B., Vimont, I., Menking, J. A., Shackleton, S. A., Baggenstos, D., Bauska,
756 T. K., Rhodes, R. H., Sperlich, P., Beaudette, R., Harth, C., Kalk, M., Brook, E. J., Fischer, H.,
757 Severinghaus, J. P., and Weiss, R. F.: Old carbon reservoirs were not important in the deglacial
758 methane budget, Science (80-), 367, 907–910, <https://doi.org/10.1126/science.aax0504>, 2020.

759 Feng, L., Palmer, P. I., Zhu, S., Parker, R. J., and Liu, Y.: Tropical methane emissions explain
760 large fraction of recent changes in global atmospheric methane growth rate, Nat. Commun., 13,
761 1378, <https://doi.org/10.1038/s41467-022-28989-z>, 2022.

762 Fischer, H., Behrens, M., Bock, M., Richter, U., Schmitt, J., Loulergue, L., Chappellaz, J., Spahni,
763 R., Blunier, T., Leuenberger, M., and Stocker, T. F.: Changing boreal methane sources and
764 constant biomass burning during the last termination, Nature, 452, 864–867,
765 <https://doi.org/10.1038/nature06825>, 2008.



766 Fisher, R. E., France, J. L., Lowry, D., Lanoisellé, M., Brownlow, R., Pyle, J. A., Cain, M.,
767 Warwick, N., Skiba, U. M., Drewer, J., Dinsmore, K. J., Leeson, S. R., Bauguitte, S. J. B.,
768 Wellpott, A., O'Shea, S. J., Allen, G., Gallagher, M. W., Pitt, J., Percival, C. J., Bower, K., George,
769 Hayman, G. D., Aalto, T., Lohila, A., Aurela, M., Laurila, T., Crill, P. M., McCalley, C. K.,
770 and Nisbet, E. G.: Measurement of the ^{13}C isotopic signature of methane emissions from northern
771 European wetlands, Global Biogeochem. Cycles, 31, 605–623,
772 <https://doi.org/10.1002/2016GB005504>, 2017.

773 France, J. L., Fisher, R. E., Lowry, D., Allen, G., Andrade, M. F., Bauguitte, S. J. B., Bower, K.,
774 Broderick, T. J., Daly, M. C., Forster, G., Gondwe, M., Helfter, C., Hoyt, A. M., Jones, A. E.,
775 Lanoisellé, M., Moreno, I., Nisbet-Jones, P. B. R., Oram, D., Pasternak, D., Pitt, J. R., Skiba, U.,
776 Stephens, M., Wilde, S. E., and Nisbet, E. G.: $\delta^{13}\text{C}$ methane source signatures from tropical
777 wetland and rice field emissions, Philos. Trans. R. Soc. A Math. Phys. Eng. Sci., 380,
778 <https://doi.org/10.1098/rsta.2020.0449>, 2022.

779 Fujita, R., Graven, H., Zazzeri, G., Hmiel, B., Petrenko, V. V., Smith, A. M., Michel, S. E., and
780 Morimoto, S.: Global Fossil Methane Emissions Constrained by Multi-Isotopic Atmospheric
781 Methane Histories, J. Geophys. Res. Atmos., 130, <https://doi.org/10.1029/2024JD041266>, 2025.

782 Ganesan, A. L., Rigby, M., Lunt, M. F., Parker, R. J., Boesch, H., Goulding, N., Umezawa, T.,
783 Zahn, A., Chatterjee, A., Prinn, R. G., Tiwari, Y. K., van der Schoot, M., and Krummel, P. B.:
784 Atmospheric observations show accurate reporting and little growth in India's methane emissions,
785 Nat. Commun., 8, 836, <https://doi.org/10.1038/s41467-017-00994-7>, 2017.

786 Ganesan, A. L., Stell, A. C., Gedney, N., Comyn-Platt, E., Hayman, G., Rigby, M., Poulter, B.,
787 and Hornbrook, E. R. C.: Spatially Resolved Isotopic Source Signatures of Wetland Methane



788 Emissions, *Geophys. Res. Lett.*, 45, 3737–3745, <https://doi.org/10.1002/2018GL077536>, 2018.

789 Guha, T., Tiwari, Y. K., Valsala, V., Lin, X., Ramonet, M., Mahajan, A., Datye, A., and Kumar,
790 K. R.: What controls the atmospheric methane seasonal variability over India?, *Atmos. Environ.*,
791 175, 83–91, <https://doi.org/10.1016/j.atmosenv.2017.11.042>, 2018.

792 Gumma, M. K.: Mapping rice areas of South Asia using MODIS multitemporal data, *J. Appl.*
793 *Remote Sens.*, 5, 053547, <https://doi.org/10.1111/1.3619838>, 2011.

794 Halder, J., Terzer, S., Wassenaar, L. I., Araguás-Araguás, L. J., and Aggarwal, P. K.: The Global
795 Network of Isotopes in Rivers (GNIR): integration of water isotopes in watershed observation and
796 riverine research, *Hydrol. Earth Syst. Sci.*, 19, 3419–3431, <https://doi.org/10.5194/hess-19-3419->
797 2015, 2015.

798 Hook, S. E., Wright, A.-D. G., and McBride, B. W.: Methanogens: Methane Producers of the
799 Rumen and Mitigation Strategies, *Archaea*, 2010, 1–11, <https://doi.org/10.1155/2010/945785>,
800 2010.

801 Hristov, A. N., Harper, M., Meinen, R., Day, R., Lopes, J., Ott, T., Venkatesh, A., and Randles,
802 C. A.: Discrepancies and Uncertainties in Bottom-up Gridded Inventories of Livestock Methane
803 Emissions for the Contiguous United States, *Environ. Sci. Technol.*, 51, 13668–13677,
804 <https://doi.org/10.1021/acs.est.7b03332>, 2017.

805 Global Network of Isotopes in Precipitation (GNIP): <https://nucleus.iaea.org/wiser>.

806 Ito, A., Patra, P. K., and Umezawa, T.: Bottom-Up Evaluation of the Methane Budget in Asia and
807 Its Subregions, *Global Biogeochem. Cycles*, 37, <https://doi.org/10.1029/2023GB007723>, 2023.

808 Jackson, R. B., Saunois, M., Bousquet, P., Canadell, J. G., Poulter, B., Stavert, A. R., Bergamaschi,



809 P., Niwa, Y., Segers, A., and Tsuruta, A.: Increasing anthropogenic methane emissions arise
810 equally from agricultural and fossil fuel sources, *Environ. Res. Lett.*, 15, 071002,
811 <https://doi.org/10.1088/1748-9326/ab9ed2>, 2020.

812 Jeffrey, L. C., Maher, D. T., Johnston, S. G., Kelaher, B. P., Steven, A., and Tait, D. R.: Wetland
813 methane emissions dominated by plant-mediated fluxes: Contrasting emissions pathways and
814 seasons within a shallow freshwater subtropical wetland, *Limnol. Oceanogr.*, 64, 1895–1912,
815 <https://doi.org/10.1002/limo.11158>, 2019.

816 Keeling, C. D.: The concentration and isotopic abundances of atmospheric carbon dioxide in rural
817 areas, *Geochim. Cosmochim. Acta*, 13, 322–334, [https://doi.org/10.1016/0016-7037\(58\)90033-4](https://doi.org/10.1016/0016-7037(58)90033-4),
818 1958.

819 Kirschke, S., Bousquet, P., Ciais, P., Saunois, M., Canadell, J. G., Dlugokencky, E. J.,
820 Bergamaschi, P., Bergmann, D., Blake, D. R., Bruhwiler, L., Cameron-Smith, P., Castaldi, S.,
821 Chevallier, F., Feng, L., Fraser, A., Heimann, M., Hodson, E. L., Houweling, S., Josse, B., Fraser,
822 P. J., Krummel, P. B., Lamarque, J.-F., Langenfelds, R. L., Le Quéré, C., Naik, V., O'Doherty, S.,
823 Palmer, P. I., Pison, I., Plummer, D., Poulter, B., Prinn, R. G., Rigby, M., Ringeval, B., Santini,
824 M., Schmidt, M., Shindell, D. T., Simpson, I. J., Spahni, R., Steele, L. P., Strode, S. A., Sudo, K.,
825 Szopa, S., van der Werf, G. R., Voulgarakis, A., van Weele, M., Weiss, R. F., Williams, J. E., and
826 Zeng, G.: Three decades of global methane sources and sinks, *Nat. Geosci.*, 6, 813–823,
827 <https://doi.org/10.1038/ngeo1955>, 2013.

828 Lauvaux, T., Giron, C., Mazzolini, M., D'Aspremont, A., Duren, R., Cusworth, D., Shindell, D.,
829 and Ciais, P.: Global assessment of oil and gas methane ultra-emitters, *Science* (80-.), 375, 557–
830 561, <https://doi.org/10.1126/science.abj4351>, 2022.



831 Lu, X., Harris, S. J., Fisher, R. E., France, J. L., Nisbet, E. G., Lowry, D., Röckmann, T., van der
832 Veen, C., Menoud, M., Schwietzke, S., and Kelly, B. F. J.: Isotopic signatures of major methane
833 sources in the coal seam gas fields and adjacent agricultural districts, Queensland, Australia,
834 *Atmos. Chem. Phys.*, 21, 10527–10555, <https://doi.org/10.5194/acp-21-10527-2021>, 2021.

835 Ma, S., Jiang, J., Huang, Y., Shi, Z., Wilson, R. M., Ricciuto, D., Sebestyen, S. D., Hanson, P. J.,
836 and Luo, Y.: Data-Constrained Projections of Methane Fluxes in a Northern Minnesota Peatland
837 in Response to Elevated CO₂ and Warming, *J. Geophys. Res. Biogeosciences*, 122, 2841–2861,
838 <https://doi.org/10.1002/2017JG003932>, 2017.

839 Masson-Delmotte, V., Zhai, P., Pirani, A., Connors, S. L., Péan, C., Berger, S., Caud, N., Chen,
840 Y., Goldfarb, L., and Gomis, M. I.: Climate change 2021: the physical science basis, *Contrib.
841 Work. Gr. I to sixth Assess. Rep. Intergov. panel Clim. Chang.*, 2,
842 <https://doi.org/10.1017/9781009157896>, 2021.

843 Menoud, M., van der Veen, C., Lowry, D., Fernandez, J. M., Bakkaloglu, S., France, J. L., Fisher,
844 R. E., Maazallahi, H., Stanisavljević, M., Nęcki, J., Vinkovic, K., Łakomiec, P., Rinne, J., Korbeń,
845 P., Schmidt, M., Defrattyka, S., Yver-Kwok, C., Andersen, T., Chen, H., and Röckmann, T.: New
846 contributions of measurements in Europe to the global inventory of the stable isotopic composition
847 of methane, *Earth Syst. Sci. Data*, 14, 4365–4386, <https://doi.org/10.5194/essd-14-4365-2022>,
848 2022.

849 Metya, A., Datye, A., Chakraborty, S., Tiwari, Y. K., Patra, P. K., and Murkute, C.: Methane
850 sources from waste and natural gas sectors detected in Pune, India, by concentration and isotopic
851 analysis, *Sci. Total Environ.*, 842, 156721, <https://doi.org/10.1016/j.scitotenv.2022.156721>, 2022.

852 Michel, S. E., Lan, X., Miller, J., Tans, P., Clark, J. R., Schaefer, H., Sperlich, P., Brailsford, G.,



853 Morimoto, S., Moosser, H., and Li, J.: Rapid shift in methane carbon isotopes suggests microbial
854 emissions drove record high atmospheric methane growth in 2020–2022, *Proc. Natl. Acad. Sci.*,
855 121, 2017, <https://doi.org/10.1073/pnas.2411212121>, 2024.

856 Miller, J. B. and Tans, P. P.: Calculating isotopic fractionation from atmospheric measurements at
857 various scales, *Tellus B Chem. Phys. Meteorol.*, 55, 207,
858 <https://doi.org/10.3402/tellusb.v55i2.16697>, 2003.

859 Naik, V., Szopa, S., Adhikary, B., Artaxo, P., Berntsen, T., Collins, W. D., Fuzzi, S., Gallardo, L.,
860 Kiendler-Scharr, A., and Klimont, Z.: Short-lived Climate Forcers, in: *Climate Change 2021 – The*
861 *Physical Science Basis*, Cambridge University Press, 817–922,
862 <https://doi.org/10.1017/9781009157896.008>, 2023.

863 Nan, Y., Tian, F., Hu, H., Wang, L., and Zhao, S.: Stable Isotope Composition of River Waters
864 across the World, *Water*, 11, 1760, <https://doi.org/10.3390/w11091760>, 2019.

865 Van Der Nat, F.-J. W. A. and Middelburg, J. J.: Effects of two common macrophytes on methane
866 dynamics in freshwater sediments, *Biogeochemistry*, 43, 79–104,
867 <https://doi.org/10.1023/A:1006076527187>, 1998.

868 Nisbet, E. G., Allen, G., Fisher, R. E., France, J. L., Lee, J. D., Lowry, D., Andrade, M. F., Bannan,
869 T. J., Barker, P., Bateson, P., Bauguitte, S. J. B., Bower, K. N., Broderick, T. J., Chibesakunda, F.,
870 Cain, M., Cozens, A. E., Daly, M. C., Ganesan, A. L., Jones, A. E., Lambakasa, M., Lunt, M. F.,
871 Mehra, A., Moreno, I., Pasternak, D., Palmer, P. I., Percival, C. J., Pitt, J. R., Riddle, A. J., Rigby,
872 M., Shaw, J. T., Stell, A. C., Vaughan, A. R., Warwick, N. J., E. Wilde, S., Team, M., Nisbet, E.
873 G., Allen, G., Fisher, R. E., France, J. L., Lee, J. D., Lowry, D., Andrade, M. F., Bannan, T. J., and
874 Barker, P.: Isotopic signatures of methane emissions from tropical fires, agriculture and wetlands:



875 the MOYA and ZWAMPS flights, *Philos. Trans. R. Soc. A Math. Phys. Eng. Sci.*, 380, 20210112,
876 <https://doi.org/10.1098/rsta.2021.0112>, 2022.

877 Nisbet, E. G., Manning, M. R., Dlugokencky, E. J., Michel, S. E., Lan, X., Röckmann, T., Denier
878 van der Gon, H. A. C., Schmitt, J., Palmer, P. I., Dyonisius, M. N., Oh, Y., Fisher, R. E., Lowry,
879 D., France, J. L., White, J. W. C., Brailsford, G., and Bromley, T.: Atmospheric Methane:
880 Comparison Between Methane's Record in 2006–2022 and During Glacial Terminations, *Global
881 Biogeochem. Cycles*, 37, <https://doi.org/10.1029/2023GB007875>, 2023.

882 Pataki, D. E., Ehleringer, J. R., Flanagan, L. B., Yakir, D., Bowling, D. R., Still, C. J., Buchmann,
883 N., Kaplan, J. O., and Berry, J. A.: The application and interpretation of Keeling plots in terrestrial
884 carbon cycle research, *Global Biogeochem. Cycles*, 17, <https://doi.org/10.1029/2001GB001850>,
885 2003.

886 Patra, P. K., Canadell, J. G., Houghton, R. A., Piao, S. L., Oh, N.-H., Ciais, P., Manjunath, K. R.,
887 Chhabra, A., Wang, T., Bhattacharya, T., Bousquet, P., Hartman, J., Ito, A., Mayorga, E., Niwa,
888 Y., Raymond, P. A., Sarma, V. V. S. S., and Lasco, R.: The carbon budget of South Asia,
889 *Biogeosciences*, 10, 513–527, <https://doi.org/10.5194/bg-10-513-2013>, 2013.

890 Peng, S., Lin, X., Thompson, R. L., Xi, Y., Liu, G., Hauglustaine, D., Lan, X., Poulter, B.,
891 Ramonet, M., Saunois, M., Yin, Y., Zhang, Z., Zheng, B., and Ciais, P.: Wetland emission and
892 atmospheric sink changes explain methane growth in 2020, *Nature*, 612, 477–482,
893 <https://doi.org/10.1038/s41586-022-05447-w>, 2022.

894 Polag, D., May, T., Müller, L., König, H., Jacobi, F., Laukenmann, S., and Keppler, F.: Online
895 monitoring of stable carbon isotopes of methane in anaerobic digestion as a new tool for early
896 warning of process instability, *Bioresour. Technol.*, 197, 161–170,



897 https://doi.org/10.1016/j.biortech.2015.08.058, 2015.

898 Rao, D. K., Bhattacharya, S. K., and Jani, R. A.: Seasonal variations of carbon isotopic
899 composition of methane from Indian paddy fields, *Global Biogeochem. Cycles*, 22, 1–5,
900 https://doi.org/10.1029/2006GB002917, 2008.

901 Rice, A. L., Gotoh, A. A., Ajie, H. O., and Tyler, S. C.: High-Precision Continuous-Flow
902 Measurement of $\delta^{13}\text{C}$ and δD of Atmospheric CH_4 , *Anal. Chem.*, 73, 4104–4110,
903 https://doi.org/10.1021/ac0155106, 2001.

904 Rice, A. L., Butenhoff, C. L., Team, D. G., Röger, F. H., Khalil, M. A. K., and Rasmussen, R.
905 A.: Atmospheric methane isotopic record favors fossil sources flat in 1980s and 1990s with recent
906 increase, *Proc. Natl. Acad. Sci.*, 113, 10791–10796, https://doi.org/10.1073/pnas.1522923113,
907 2016.

908 Rogelj, J., den Elzen, M., Höhne, N., Fransen, T., Fekete, H., Winkler, H., Schaeffer, R., Sha, F.,
909 Riahi, K., and Meinshausen, M.: Paris Agreement climate proposals need a boost to keep warming
910 well below 2 °C, *Nature*, 534, 631–639, https://doi.org/10.1038/nature18307, 2016.

911 Rosentreter, J. A., Borges, A. V., Deemer, B. R., Holgerson, M. A., Liu, S., Song, C., Melack, J.,
912 Raymond, P. A., Duarte, C. M., Allen, G. H., Olefeldt, D., Poulter, B., Battin, T. I., and Eyre, B.
913 D.: Half of global methane emissions come from highly variable aquatic ecosystem sources, *Nat.*
914 *Geosci.*, 14, 225–230, https://doi.org/10.1038/s41561-021-00715-2, 2021.

915 Saunois, M., Martinez, A., Poulter, B., Zhang, Z., Raymond, P. A., Regnier, P., Canadell, J. G.,
916 Jackson, R. B., Patra, P. K., Bousquet, P., Ciais, P., Dlugokencky, E. J., Lan, X., Allen, G. H.,
917 Bastviken, D., Beerling, D. J., Belikov, D. A., Blake, D. R., Castaldi, S., Crippa, M., Deemer, B.



918 R., Dennison, F., Etiope, G., Gedney, N., Höglund-Isaksson, L., Holgerson, M. A., Hopcroft, P.
919 O., Hugelius, G., Ito, A., Jain, A. K., Janardanan, R., Johnson, M. S., Kleinen, T., Krummel, P. B.,
920 Lauerwald, R., Li, T., Liu, X., McDonald, K. C., Melton, J. R., Mühle, J., Müller, J., Murguia-
921 Flores, F., Niwa, Y., Noce, S., Pan, S., Parker, R. J., Peng, C., Ramonet, M., Riley, W. J., Rocher-
922 Ros, G., Rosentreter, J. A., Sasakawa, M., Segers, A., Smith, S. J., Stanley, E. H., Thanwerdas, J.,
923 Tian, H., Tsuruta, A., Tubiello, F. N., Weber, T. S., van der Werf, G. R., Worthy, D. E. J., Xi, Y.,
924 Yoshida, Y., Zhang, W., Zheng, B., Zhu, Q., Zhu, Q., and Zhuang, Q.: Global Methane Budget
925 2000–2020, *Earth Syst. Sci. Data*, 17, 1873–1958, <https://doi.org/10.5194/essd-17-1873-2025>,
926 2025.

927 Schaefer, H. and Whiticar, M. J.: Potential glacial-interglacial changes in stable carbon isotope
928 ratios of methane sources and sink fractionation, *Global Biogeochem. Cycles*, 22, 1–18,
929 <https://doi.org/10.1029/2006GB002889>, 2008.

930 Schaefer, H., Fletcher, S. E. M., Veidt, C., Lassey, K. R., Brailsford, G. W., Bromley, T. M.,
931 Dlugokencky, E. J., Michel, S. E., Miller, J. B., Levin, I., Lowe, D. C., Martin, R. J., Vaughn, B.
932 H., and White, J. W. C.: A 21st-century shift from fossil-fuel to biogenic methane emissions
933 indicated by $^{13}\text{CH}_4$, *Science* (80-), 352, 80–84, <https://doi.org/10.1126/science.aad2705>, 2016.

934 Schaeffer, R., Schipper, E. L. F., Ospina, D., Mirazo, P., Alencar, A., Anvari, M., Artaxo, P.,
935 Biresselioglu, M. E., Blome, T., Boeckmann, M., Brink, E., Broadgate, W., Bustamante, M., Cai,
936 W., Canadell, J. G., Cardinale, R., Chidichimo, M. P., Ditlevsen, P., Eicker, U., Feron, S., Fikru,
937 M. G., Fuss, S., Gaye, A. T., Gustafsson, Ö., Harring, N., He, C., Hebden, S., Heilemann, A.,
938 Hirota, M., Janardhanan, N., Juhola, S., Jung, T. Y., Kejun, J., Kilkış, Ş., Kumarasinghe, N.,
939 Lapola, D., Lee, J.-Y., Levis, C., Lusambili, A., Maasakkers, J. D., MacIntosh, C., Mahmood, J.,



940 Mankin, J. S., Marchegiani, P., Martin, M., Mukherji, A., Muñoz-Erickson, T. A., Niazi, Z.,
941 Nyangon, J., Pandipati, S., Perera, A. T. D., Persad, G., Persson, Å., Redman, A., Riipinen, I.,
942 Rockström, J., Roffe, S., Roy, J., Sakschewski, B., Samset, B. H., Schlosser, P., Sharifi, A., Shih,
943 W.-Y., Sioen, G. B., Sokona, Y., Stammer, D., Suk, S., Thiam, D., Thompson, V., Tullos, E., van
944 Westen, R. M., Vargas Falla, A. M., Vecellio, D. J., Worden, J., Wu, H. C., Xu, C., Yang, Y.,
945 Zachariah, M., Zhang, Z., and Ziervogel, G.: Ten new insights in climate science 2024, *One Earth*,
946 101285, <https://doi.org/10.1016/j.oneear.2025.101285>, 2025.

947 Schmitt, J., Seth, B., Bock, M., van der Veen, C., Möller, L., Sapart, C. J., Prokopiou, M., Sowers,
948 T., Röckmann, T., and Fischer, H.: On the interference of Kr during carbon isotope analysis of
949 methane using continuous-flow combustion–isotope ratio mass spectrometry, *Atmos. Meas. Tech.*,
950 6, 1425–1445, <https://doi.org/10.5194/amt-6-1425-2013>, 2013.

951 Schütz, H., Seiler, W., and Conrad, R.: Processes involved in formation and emission of methane
952 in rice paddies, *Biogeochemistry*, 7, 33–53, <https://doi.org/10.1007/BF00000896>, 1989.

953 Schwietzke, S., Sherwood, O. A., Bruhwiler, L. M. P., Miller, J. B., Etiope, G., Dlugokencky, E.
954 J., Michel, S. E., Arling, V. A., Vaughn, B. H., White, J. W. C., and Tans, P. P.: Upward revision
955 of global fossil fuel methane emissions based on isotope database, *Nature*, 538, 88–91,
956 <https://doi.org/10.1038/nature19797>, 2016.

957 Shen, L., Jacob, D. J., Gautam, R., Omara, M., Scarpelli, T. R., Lorente, A., Zavala-Araiza, D.,
958 Lu, X., Chen, Z., and Lin, J.: National quantifications of methane emissions from fuel exploitation
959 using high resolution inversions of satellite observations, *Nat. Commun.*, 14, 4948,
960 <https://doi.org/10.1038/s41467-023-40671-6>, 2023.

961 Sherwood, O. A., Schwietzke, S., Arling, V. A., and Etiope, G.: Global Inventory of Gas



962 Geochemistry Data from Fossil Fuel, Microbial and Burning Sources, version 2017, *Earth Syst.*
963 *Sci. Data*, 9, 639–656, <https://doi.org/10.5194/essd-9-639-2017>, 2017.

964 Singh, A., Kuttippurath, J., Abhishek, K., Mallick, N., Raj, S., Chander, G., and Dixit, S.:
965 Biogenic link to the recent increase in atmospheric methane over India, *J. Environ. Manage.*, 289,
966 112526, <https://doi.org/10.1016/j.jenvman.2021.112526>, 2021.

967 Smartt, A. D., Brye, K. R., and Norman, R. J.: Methane Emissions from Rice Production in the
968 United States — A Review of Controlling Factors and Summary of Research, in: *Greenhouse*
969 *Gases*, InTech, <https://doi.org/10.5772/62025>, 2016.

970 Stavert, A. R., Saunois, M., Canadell, J. G., Poulter, B., Jackson, R. B., Regnier, P., Lauerwald,
971 R., Raymond, P. A., Allen, G. H., Patra, P. K., Bergamaschi, P., Bousquet, P., Chandra, N., Ciais,
972 P., Gustafson, A., Ishizawa, M., Ito, A., Kleinen, T., Maksyutov, S., McNorton, J., Melton, J. R.,
973 Müller, J., Niwa, Y., Peng, S., Riley, W. J., Segers, A., Tian, H., Tsuruta, A., Yin, Y., Zhang, Z.,
974 Zheng, B., and Zhuang, Q.: Regional trends and drivers of the global methane budget, *Glob.*
975 *Chang. Biol.*, 28, 182–200, <https://doi.org/10.1111/gcb.15901>, 2022.

976 Still, C. J., Berry, J. A., Collatz, G. J., and DeFries, R. S.: Global distribution of C3 and C4
977 vegetation: Carbon cycle implications, *Global Biogeochem. Cycles*, 17,
978 <https://doi.org/10.1029/2001GB001807>, 2003.

979 Thanwerdas, J., Saunois, M., Berchet, A., Pison, I., and Bousquet, P.: Investigation of the renewed
980 methane growth post-2007 with high-resolution 3-D variational inverse modeling and isotopic
981 constraints, *Atmos. Chem. Phys.*, 24, 2129–2167, <https://doi.org/10.5194/acp-24-2129-2024>,
982 2024.



983 Tiwari, Y. K., Guha, T., Valsala, V., Lopez, A. S., Cuevas, C., Fernandez, R. P., and Mahajan, A.
984 S.: Understanding atmospheric methane sub-seasonal variability over India, *Atmos. Environ.*, 223,
985 117206, <https://doi.org/10.1016/j.atmosenv.2019.117206>, 2020.

986 Tyler, S. C., Zimmerman, P. R., Cumberbatch, C., Greenberg, J. P., Westberg, C., and Darlington,
987 J. P. E. C.: Measurements and interpretation of $\delta^{13}\text{C}$ of methane from termites, rice paddies, and
988 wetlands in Kenya, *Global Biogeochem. Cycles*, 2, 341–355,
989 <https://doi.org/10.1029/GB002i004p00341>, 1988.

990 Vernooij, R., Dusek, U., Popa, M. E., Yao, P., Shaikat, A., Qiu, C., Winiger, P., van der Veen, C.,
991 Eames, T. C., Ribeiro, N., and van der Werf, G. R.: Stable carbon isotopic composition of biomass
992 burning emissions – implications for estimating the contribution of C3 and C4 plants, *Atmos.*
993 *Chem. Phys.*, 22, 2871–2890, <https://doi.org/10.5194/acp-22-2871-2022>, 2022.

994 Villa, J. A., Ju, Y., Stephen, T., Rey-Sanchez, C., Wrighton, K. C., and Bohrer, G.: Plant-mediated
995 methane transport in emergent and floating-leaved species of a temperate freshwater mineral-soil
996 wetland, *Limnol. Oceanogr.*, 65, 1635–1650, <https://doi.org/10.1002/lno.11467>, 2020.

997 Whiticar, M. and Schaefer, H.: Constraining past global tropospheric methane budgets with carbon
998 and hydrogen isotope ratios in ice, *Philos. Trans. R. Soc. A Math. Phys. Eng. Sci.*, 365, 1793–
999 1828, <https://doi.org/10.1098/rsta.2007.2048>, 2007.

1000 Whiticar, M. ., Faber, E., and Schoell, M.: Biogenic methane formation in marine and freshwater
1001 environments: CO₂ reduction vs. acetate fermentation—Isotope evidence, *Geochim. Cosmochim.*
1002 *Acta*, 50, 693–709, [https://doi.org/10.1016/0016-7037\(86\)90346-7](https://doi.org/10.1016/0016-7037(86)90346-7), 1986.

1003 Whiticar, M. J.: Carbon and hydrogen isotope systematics of bacterial formation and oxidation of



1004 methane, *Chem. Geol.*, 161, 291–314, [https://doi.org/10.1016/S0009-2541\(99\)00092-3](https://doi.org/10.1016/S0009-2541(99)00092-3), 1999.

1005 Yao, P., Belec, K., Holmstrand, H., Balacky, J., Salam, A., Budhavant, K., Manoj, M.R., Joy, K.S.,

1006 Hossain, M.A., Singh, A., Patel, A., Rastogi, N., Mallik, C., Ram, K., Singh, G.K., Gustafsson,

1007 Ö., Isotopic values of major methane sources in South Asia and worldwide, *Bolin Centre Database*,

1008 <https://bolin.su.se/data/draft?id=13645&token=f0770bfd-210f-4a51-a9bd-a355467058a4>, 2025.

1009 Yao, P., Huang, R.-J., Ni, H., Kairys, N., Yang, L., Meijer, H. A. J., and Dusek, U.: ^{13}C signatures

1010 of aerosol organic and elemental carbon from major combustion sources in China compared to

1011 worldwide estimates, *Sci. Total Environ.*, 810, 151284,

1012 <https://doi.org/10.1016/j.scitotenv.2021.151284>, 2022.

1013 Zavala-Araiza, D., Lyon, D. R., Alvarez, R. A., Davis, K. J., Harriss, R., Herndon, S. C., Karion,

1014 A., Kort, E. A., Lamb, B. K., Lan, X., Marchese, A. J., Pacala, S. W., Robinson, A. L., Shepson,

1015 P. B., Sweeney, C., Talbot, R., Townsend-Small, A., Yacovitch, T. I., Zimmerle, D. J., and

1016 Hamburg, S. P.: Reconciling divergent estimates of oil and gas methane emissions, *Proc. Natl.*

1017 *Acad. Sci.*, 112, 15597–15602, <https://doi.org/10.1073/pnas.1522126112>, 2015.

1018 Zhang, Z., Poulter, B., Knox, S., Stavert, A., McNicol, G., Fluet-Chouinard, E., Feinberg, A.,

1019 Zhao, Y., Bousquet, P., Canadell, J. G., Ganesan, A., Hugelius, G., Hurt, G., Jackson, R. B., Patra,

1020 P. K., Saunois, M., Höglund-Isaksson, L., Huang, C., Chatterjee, A., and Li, X.: Anthropogenic

1021 emission is the main contributor to the rise of atmospheric methane during 1993–2017, *Natl. Sci.*

1022 *Rev.*, 9, <https://doi.org/10.1093/nsr/nwab200>, 2022.

1023 Zhao, J., Ciais, P., Chevallier, F., Canadell, J. G., van der Velde, I. R., Chuvieco, E., Chen, Y.,

1024 Zhang, Q., He, K., and Zheng, B.: Enhanced CH_4 emissions from global wildfires likely due to

1025 undetected small fires, *Nat. Commun.*, 16, 804, <https://doi.org/10.1038/s41467-025-56218-w>,



1026 2025.

1027